IPP-Report

MAX-PLANCK-INSTITUT
FÜR PLASMAPHYSIK

Marcel Schmid

Plasma-assisted Conversion of CO_2 – Process Design and Techno-economic Evaluation

IPP 2024-09
April 2024

MAX PLANCK INSTITUTE
FOR PLASMA PHYSICS

Plasma-assisted Conversion of CO_2 – Process Design and Techno-economic Evaluation

Author:	Marcel Schmid
Supervisors:	Florian Kerscher | Technical University of Munich Christian Kiefer | Max Planck Institute for Plasma Physics Ante Hecimovic | Max Planck Institute for Plasma Physics
Date:	12.11.2023

Lehrstuhl für Energiesysteme

Title of Term Paper	Plasma-assisted Conversion of CO_2 – Process Design and Techno-economic Evaluation
Author:	Marcel Schmid
Enrolment number:	03768988
Supervisor:	Dr.-Ing. Florian Kerscher
Assigned by:	Prof. Dr.-Ing. Hartmut Spliethoff Technical University of Munich Chair of Energy Systems Boltzmannstr. 15 DE-85748 Garching
Assigned:	12.05.2023
Handed in:	12.11.2023

Statutory Declaration

I hereby declare that I have prepared the present work independently and without help of others. Thoughts and quotes that have been taken over directly or indirectly from other sources are marked as such. This work has not been submitted to any examining authority in the same or similar form and has not been published yet.

I hereby agree that the work can be made available by the Institute of Energy Systems and the Max Planck Institute for Plasma Physics to the public.

Fukuoka, the 06.11.2023

Signature

Abstract

Mitigating climate change necessitates the development of new production pathways for value-added chemicals. Carbon monoxide (CO) is a crucial feedstock for this purpose. One promising technology for the production of CO is the conversion of carbon dioxide (CO_2) by plasma-assisted processes that are powered with renewable energies. Due to their high potential for flexible operation and high theoretical efficiencies, plasma processes can exceed the limitations of traditional thermal conversion approaches. This work focusses on the process design and modelling of an industrial CO_2 conversion process based on microwave plasma reactor using Aspen Plus V12. The simulation data are analyzed to evaluate the techno-economic key performance indicators of the process. The results indicate that CO can be produced with an overall efficiency of approximately 17% for the present reactor design. Notably, the microwave plasma reactor accounts for at least 85% of the total energy demand at the investigated operating points. The levelized cost of CO production (LCOP) stands at 4.44 €/kg_{CO} at the base case (0.20 €/kWh), but it can decrease to as low as 0.93 €/kg_{CO} in the proposed ideal scenario. This cost is heavily depended on electricity prices and annual operating hours. To enhance the economic competitiveness of microwave plasma-based CO_2 conversion, achieving higher plasma efficiencies and addressing waste heat utilization are crucial. Additionally, the development of larger reactor concepts can lead to economies of scale and reduced investment costs.

Key Words: techno-economic evaluation, CO_2 conversion, microwave plasma, process simulation

Table of Contents

List of Figures

List of Tables

Abbreviations

Abbreviation	Meaning
CAPEX	Capital Expenditures
DBD	Dielectric Barrier Discharge
EPC	Electrical Power Consumption
FCI	Fixed-Capital Investment
GA	Gliding Arc
GDE	Gas Diffusion Electrode
GHG	Greenhouse Gas
HRSG	Heat-Recovery Steam Generator
LCOP	Levelized Costs of Product
LTE	Local Thermodynamic Equilibrium
MW	Microwave
OL	Operating Labor
OPEX	Operational Expenditures
P2X	Power-to-X
PFD	Process Flow Diagram
PSA	Pressure Swing Adsorption
SEI	Specific Energy Input
TPC	Total Product Costs
TPEC	Total Purchased Equipment Costs
TSA	Temperature Swing Adsorption
WC	Working Capital

Notation

Latin Symbols

Symbol	Unit	Explanation
C_A	€	Costs for equipment A
C_B	€	Costs for equipment B
C_1	€	Costs at time 1
C_2	€	Costs at time 2
c_{OL}	$\frac{€}{h}$	Specific operating labor costs
c_{RES}	$\frac{€}{kg} / \frac{€}{kWh}$	Specific costs for raw materials and utilities
ΔH_r	$\frac{kJ}{mol}$	Heat of reaction
i	-	Interest rate
$\dot{n}_{CO_2,Out}$	$\frac{mol}{s}$	Molar flow of CO_2 out of the reactor
$\dot{n}_{Total,Out}$	$\frac{mol}{s}$	Total molar flow out of the reactor
$\dot{n}_{CO_2,In}$	$\frac{mol}{s}$	Molar flow of CO_2 into the reactor
$\dot{n}_{CO_2,Feed}$	$\frac{mol}{s}$	Molar flow of CO_2 in feed gas
$\dot{n}_{CO,Product}$	$\frac{mol}{s}$	Molar flow of CO in the product stream
N_{OL}	-	Number of operators
$\dot{m}_{CO}$	$\frac{kg}{s}$	Mass flow of CO
P_{In}	W	Injected power
P_E^i	kW	Electric power demand of single equipment or process unit
$P_{E,Total}$	kW	Total electric power demand
r	-	Exponent for equipment scaling

S_A	$\mathrm{kW/m^2/m^3}$	Capacity or size of equipment A
S_B	$\mathrm{kW/m^2/m^3}$	Capacity or size of equipment B
t	a	Plant lifetime
t_{OP}	$\frac{\mathrm{h}}{\mathrm{a}}$	Annual operating time
T_{Out}	°C	Reactor outlet temperature (after quench)

Greek Symbols

Symbol	Unit	Explanation
η_{CO_2}	%	Carbon efficiency
$\eta_{\mathrm{MW\ Source}}$	%	Efficiency of the microwave source
η_{Plasma}	%	Plasma efficiency
η_{Total}	%	Total efficiency of the process
χ_{CO_2}	%	Conversion rate

1 Introduction

1.1 Motivation

The anthropogenic global warming – mainly caused by the emission of greenhouse gases (GHG) such as CO_2 – provokes various ecological, social, and economic issues. To overcome this problem the concentration of CO_2 in the atmosphere must be limited or even reduced urgently, since there is a rapidly closing window of opportunity to achieve the required net zero GHG emissions. Therefore, the demand for decarbonization is present in all industrial sectors which contribute a major part of the anthropogenic GHG emissions. [1]

As the chemical and in particular the petrochemical sector are one of the biggest emitters of CO_2 [2], there is a high potential for new technologies and production routes aiming to mitigate these emissions. Power-to-X (P2X) processes are one of those new production routes. Driven by renewable energies it is not only possible to produce value-added chemicals and fuels with net-zero emissions but also enable the coupling of the electricity sector, the mobility sector and chemical industry. One feedstock which is of major interest for the chemical industry is so-called syngas, a mixture of H_2 and CO. While green hydrogen can be produced, for example, via water electrolysis, the sustainable provision of CO is challenging. An environmentally attractive CO source is atmospheric CO_2. Captured directly from the air, it can be converted into CO and O_2. Conventional thermo-catalytic processes, however, have to deal with several issues regarding energy efficiency, heat integration and operation dynamics of the CO_2 conversion. In contrast to that, plasma-based processes show a high potential for an energy-efficient and dynamic conversion pathway based on renewable electricity. [3] Among other methods, specifically microwave (MW) plasmas have shown in experiments that efficient conversion of CO_2 is achievable in a small-scale reactor. [4] Nevertheless, there are currently no large-scale process plants in existence that integrate the plasma reactor into a comprehensive system that enables industrial utilization of the produced CO. Therefore, the potential of industrial application is being evaluated in the scope of this work.

1.2 Task

The working group *Plasmas for Gas Conversion* of the *Max Planck Institute for Plasma Physics* is currently working on a CO_2 conversion reactor based on a MW plasma. This reactor, a so-called plasma torch, has been investigated in an experimental setup on a laboratory scale. [5–7]

The aim of this term paper is the integration of this type of plasma reactor into a complete system and the process design for an industrial application. In order to achieve this, the following tasks are obtained:

1. Process design
    a. Identification of required unit operations for an industrial large-scale plant including the evaluation of up- and downstream processes.
    b. Investigation of potential technologies which could be applied in unit operations including a state-of-the-art review.
2. Process simulation
    a. Implementation of the developed process in the simulation software *Aspen Plus V12* and execution of steady-state simulations.
    b. Modelling of the MW plasma reactor on basis of the experimental data provided by the working group of the *Max Planck Institute for Plasma Physics.*
3. Techno-economic analysis
    a. Evaluation of the simulation results by means of technological and economic key performance indicators (KPI).
    b. Investigation of optimization potential and analysis of sensitivities.

1.3 Outline

Following the introduction, in chapter 2 the fundamentals for the plasma-based CO_2 conversion process are briefly explained and the state of the art of relevant technologies is presented. A general introduction to plasma properties and classifications is provided and relevant plasma-based technologies are explained. Moreover, different gas separation technologies that could potentially be applied in a plasma-based conversion process are described. In chapter 3, the fundamentals and the methodology for the design and simulation of the plasma-based CO_2 conversion process as well as the techno-economic evaluation are explained. Moreover, the data basis, boundary conditions, simplifications as well as made assumptions are illustrated. Subsequently, in chapter 4 the results of the techno-economic evaluation are presented, and sensitivity analyses are conducted to demonstrate the potential for cost reduction. Finally, chapter 5 summarizes the methods applied and the key findings of this thesis. Additionally, an outlook to possible future research is provided.

2 Fundamentals and State of the Art

In this chapter the required fundamentals for the plasma-based CO_2 conversion process are briefly explained and the state of the art of relevant technologies is presented. First, an introduction to plasmas and plasma-based technologies is given in chapters 2.1 and 2.2. Second, different gas separation technologies which potentially be applied in a plasma-based conversion process are described in chapter 2.3.

2.1 Plasma Fundamentals

Plasma which is often referred to as fourth state of matter is ionized gas. In ionized gases at least some electrons are not further bound to atoms or molecules due to their high energy. Plasmas are particularly attractive for conversion processes due to their possibility to achieve higher energy densities compared to traditional processes and their high concentration of reactive species such as electrons, ions, radicals, and excited species. Additionally, these reactive species can be already provided at low bulk temperatures since plasmas can be operated far from thermodynamic equilibrium. [8]

When regarding artificial plasmas, which are the ones relevant for technical applications, two types can be distinguished. On the one hand, there are the high-temperature plasmas, which are in general fully ionized plasmas and, for instance, used in nuclear fusion processes. On the other hand, there are low-temperature plasmas (also known as gas discharges) which are usually characterized by a low degree of ionization. The latter, low-temperature plasmas, can be further subdivided whether they are in a (local) thermodynamic equilibrium (LTE) or not. Since there a various different species present in a plasma their energy distribution (or temperature) may differ from each other. If this is the case, the plasma is far from LTE and usually called *non-LTE* or *non-thermal plasma*. However, if LTE exist the plasma is classified as *LTE plasma* or *thermal plasma*. At times, the transitional section between *non-thermal* and *thermal plasmas* is categorized as a distinct plasma type, so-called *warm plasma*. This type of plasma shares the properties of both the above, a high level of non-equilibrium and a relatively high energy density resulting in beneficial conditions for gas conversion processes. [4]

In general plasmas can be generated when enough energy is supplied to a neutral gas. This can be achieved, for example, by thermal energy from exothermic reactions or through adiabatic compression. For technical application the generation and sustainment of low-temperature plasmas is mostly done by means of an electric field. The electric field accelerates the free charge carriers and causes collisions with other particles leading either to the creation of new charged particles or the loss of existing charge carriers. In this way, under certain operating conditions, it is possible to establishment of a stable, steady-state plasma. [9]

2.2 Technologies for Plasma-assisted CO_2 Conversion

The field of CO_2 conversion is currently very dynamic due to the urgency of maintaining or even decreasing the CO_2 concentration in the atmosphere to mitigate global warming. A lot of effort is put into the research of CO_2 conversion technologies such as electrochemical [10], thermochemical [11, 12], photochemical [13] or biochemical conversion processes [14]. Yet, none of the technologies in development seems to be clearly superior. However, the utilization of plasma reactors is promising due to the advantageous conditions described earlier. Theoretically, there is no need to heat the CO_2 to extremely high temperatures since the gas is made reactive by the high energetic electrons. Additionally, because plasma reactors are electrically powered they can be easily switched on and of allowing a very flexible operation mode making them also suitable for peak shaving and grid stabilization applications. [4]

When splitting pure CO_2, besides the oxygen (O_2), only two possible carbon-containing products are formed: Carbon monoxide (CO) or solid carbon. In typical plasma reactors, there is no carbon deposition, meaning that the selectivity towards CO is 100%. The resulting reaction is given in equation (2-1). A minimum energy of 2.93 eV per molecule is required[1] [5] as shown in equation (2-1). This equals approximately 283 kJ/mol. The complex reaction mechanisms and the various side reactions are not discussed in this thesis. Further information can be found in the work of Bogaerts et al. [15].

$$CO_2 \rightarrow O_2 + CO \qquad \Delta H_R = 2.93\ eV \tag{2-1}$$

By means of the heat of the reaction ΔH_R, the energy efficiency of the plasma η_{Plasma}, can be calculated as follows. [5]

$$\eta_{\mathrm{Plasma}} = \chi_{CO_2} * \frac{\Delta H_R}{SEI} \tag{2-2}$$

Where SEI represents the specific energy input to the plasma, expressed in power per flow, and χ_{CO2} stands for the conversion rate of CO_2. For the calculation of the SEI, the total flow of CO_2 through the reactor is used and not only the gas flow which effectively interacts with the plasma. The conversion rate χ_{CO2} can be determined using equation (2-3), which depends on the molar flow of CO_2, $\dot{n}_{CO2,Out}$, and the total molar flow of the effluent, $\dot{n}_{\mathrm{Total,out}}$. Further details can be found in [5].

$$\chi_{CO_2} = 1 - \frac{\dot{n}_{CO_2,Out}}{\dot{n}_{CO_2,In}} = \frac{1 - \frac{\dot{n}_{CO_2,Out}}{\dot{n}_{Total,out}}}{1 + \frac{\dot{n}_{CO_2,Out}}{2\dot{n}_{Total,Out}}} \tag{2-3}$$

To provide the energy for creating plasma and initiating the conversion reaction, several promising technologies have been identified for their energy efficiency and CO_2 conversion proficiency. Presently, the three main technologies under extensive research are

[1] The value of 2,93 eV per molecule refers to the overall required energy as a result of the combination of different reactions taking place. More details can be found in [5].

microwave discharges (MW), dielectric barrier discharges (DBD) and gliding arc discharges (GA) [16]. An overview of the performance of these plasma types is provided in Figure 2-1. Additionally, the efficiency target and the thermal equilibrium limit are indicated. It is debated that a minimum efficiency of 60% is required for plasma-based conversion technologies to be considered competitive in producing the CO component of syngas. [4]

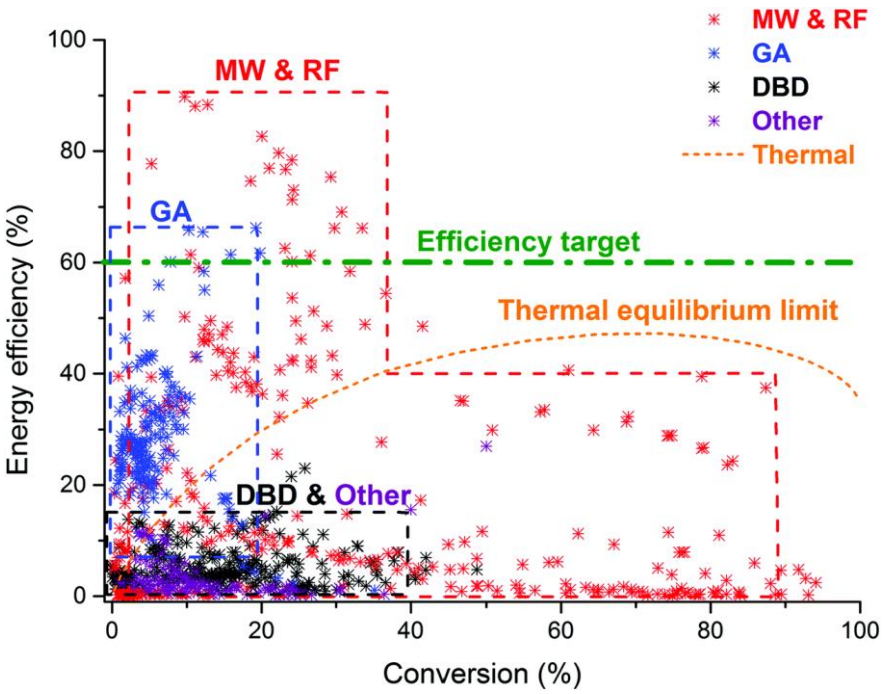

Figure 2-1: Comparison of literature data for CO_2 splitting in the different plasma types, showing the plasma energy efficiency as a function of the conversion. MW & RF: Microwave and radiofrequency, GA: Gliding arc, DBD: Dielectric barrier discharge. [4]

2.2.1 Microwave Discharge Reactors

MW plasma reactors are operated without electrodes since the energy is provided by electromagnetic radiation with frequencies between 300 MHz and 10 GHz. [17] A schematic reactor assembly is given in Figure 2-2. The main component is the power supply and the MW head, which together form the *MW source* (1). The maximum output power of commercially available systems operating at 915 MHz is 100 kW. Higher frequency MW sources can only achieve lower power outputs, for example, 15 kW at 2,45 GHz. The *isolator* (2) is required to protect the magnetron form the reflected MW field. The *impedance tuner* (3) allows to minimize the reflected MW power and enables an efficient energy transfer to the plasma. Number (4) shows the general *reactor assembly*. Gas is directed through a microwave-transparent quartz tube that allows microwave (MW) radiation to pass through. The gas discharge is initiated at the intersection with a rectangular waveguide, where the MW energy is absorbed by the plasma. In some reactors a *moveable plunger* (5) is installed to position the electromagnetic wave such that a local electric field maximum is located at the center of the plasma zone. [3]

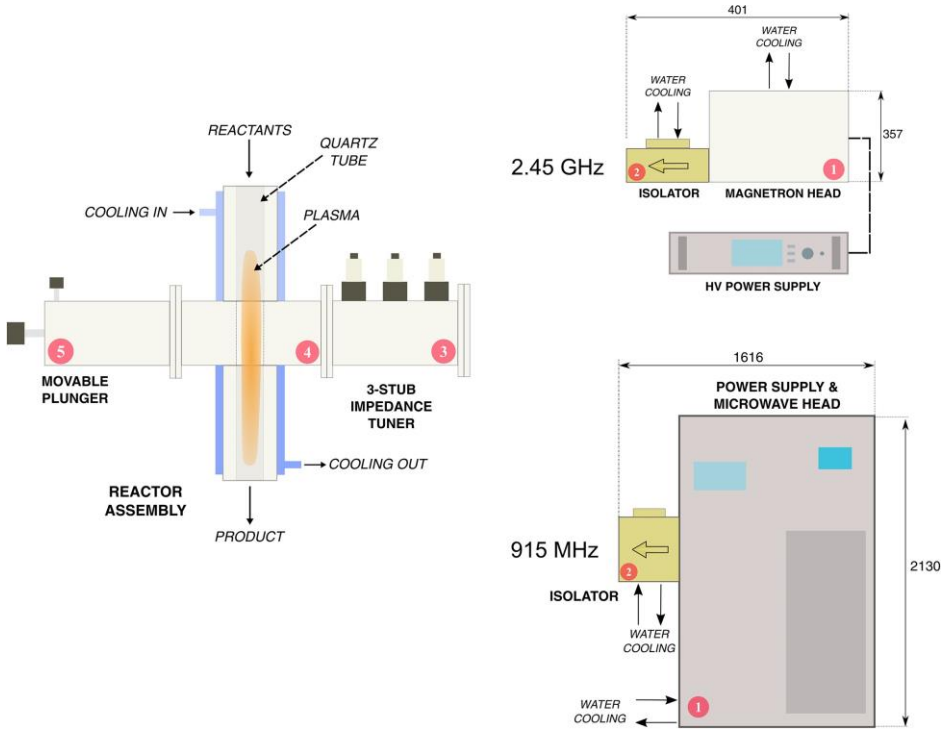

Figure 2-2: Schematic reactor assembly of a microwave plasma reactor including the main components [3]

This basic reactor assembly has been further developed in order to improve the performance. For instance, it was shown that fast cooling or quenching of the reaction gas with high temperature gradients (> 10^7 K/s) at the outlet inhibits CO_2 recombination reactions. This leads to higher conversion rates at the same specific energy input. Several methods such as forced mixing of hot gas from the plasma with the surrounding colder gas by means of a nozzle at the reactor outlet and water-cooled channels have been successfully tested. In addition, special flow configurations that increase the turbulence in the reactor and lead to better gas mixing and cooling may be capable of further increase the conversion and energy efficiency of MW plasma reactors. [6, 7] Advanced designs of current research are shown in Figure 2-3.

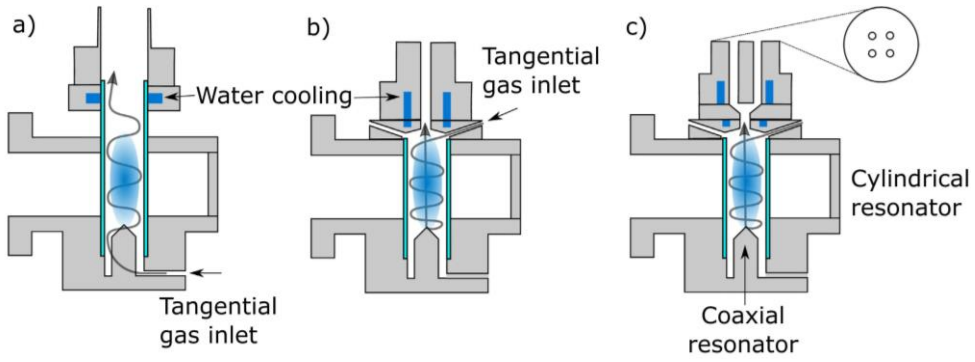

Figure 2-3: Schematic microwave plasma reactor in a) standard configuration, b) reverse vortex with a single gas channel in the effluent c) reverse vortex with 4 gas channels in the effluent [7]

As depicted in Figure 2-1, MW-based CO_2 dissociation can achieve relatively high energy efficiencies and conversion rates. Even though the both cannot be achieved simultaneously yet, MW discharges seems one of the most promising plasma technologies for CO_2 conversion [5]. However, when it comes to the scale-up of MW plasma reactor for large-scale applications other types of plasma reactor may be advantageous for now since the maximum power output of available MW sources is relatively low as described earlier.

2.2.2 Dielectric Barrier Discharge Reactors

DBD are known for over 150 years now and are already applied in large-scale industrial applications today such as ozone generation. DBD reactors can be easily scaled-up up to megawatts of power input and are mostly operated at frequencies in the range of kHz to MHz. [18] The basic configuration of a DBD reactor consists of two electrodes (planar or cylindrical) as shown in Figure 2-4. At least one of the electrodes is covered by a dielectric barrier, for example, quartz. The barrier reduces the transport of charge carriers and thus prevents the formation of arcs. The reactor is usually operated at reduced or atmospheric pressure. The efficiency of DBD reactors for CO_2 conversion is relatively low when compared to other technologies (refer to Figure 2-1). The performance might be improved by applying packing materials in the gap between the electrodes. With the so-called packed bed DBD reactors, it is possible to create an enhanced electric field at the same power input. Nevertheless, their energy efficiency is still not very high which makes it unlikely that DBD is the superior technology compared to MW or GA discharges. [4, 17]

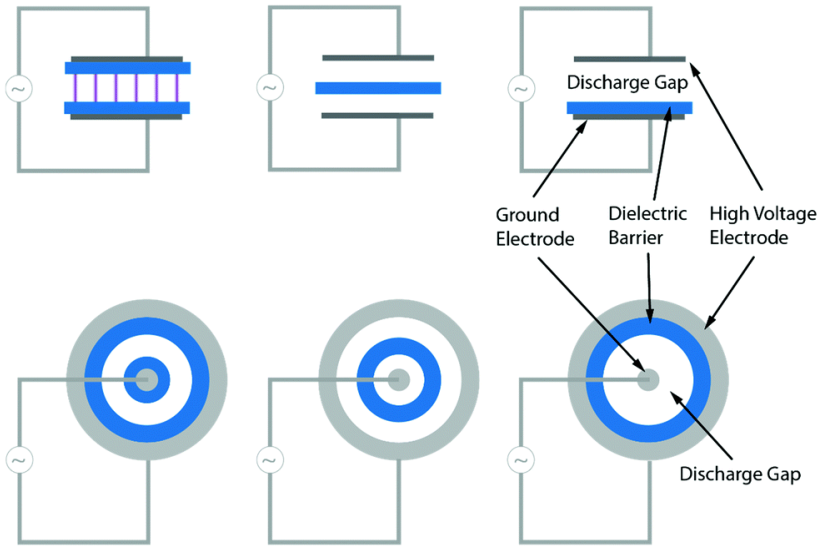

Figure 2-4: Basic planar (top) and cylindrical (bottom) dielectric barrier discharge configurations [4]

2.2.3 Gliding Arc Discharge Reactors

GA discharge reactors consist of two flat, diverging electrodes. Due to the potential between the electrodes an arc is initiated at the narrowest gap creating a plasma. The gas which is flowing through the gap is causing the arc to be pushed towards a larger interelectrode gap until the distance between the electrodes reaches a critical length and the arc extinguishes. This process is repeated continuously, starting again with the creation of an arc at the narrowest gap. Since a large fraction of the process gas does not pass through the arc because of the unfavorable two-dimensional design, the conversion rate is relatively low. Therefore, advanced three-dimensional designs have been developed known as plasmatron or rotating GA. This design allows a longer residence time by introducing the gas at a tangential inlet creating a (reverse) vortex around the electrodes. [17] A schematic design of both the original and the plasmatron GA is shown in Figure 2-5.

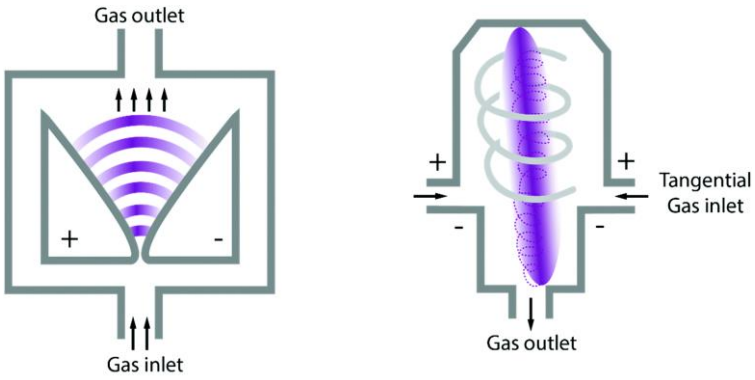

Figure 2-5: Schematic design of the original GA (left) and the plasmatron GA (right) configuration [4]

2.3 Gas Separation Processes

To attain the desired gas specification and purity, separation processes are a fundamental part of chemical plants. In the process of plasma-based CO_2 conversion, gas separation is indispensable to facilitate CO utilization in subsequent processes. As outlined in chapter 2.2, as the gas exits the reactor, it is composed of three elements: CO_2 (which was not dissociated), CO, and O_2. The challenge of separating three gases is specific to plasma-based conversion technologies. By comparison, in solid-oxide electrolysis cells, only two gases (CO, CO_2) need to be separated [19], which is much less challenging. This makes separation of three gases a major disadvantage of plasma conversion technologies. In the following sections, a variety of separation technologies is presented. Nonetheless, the review solely encompasses potential options that have been discussed in the literature as suitable.

First, there are gas separation technologies based on adsorption. Adsorption is defined as the process by which atoms or molecules from a fluid phase adhere to the surface of a solid phase. The material on which the particles are binding at is also known as adsorbent and is usually a porous medium with a large surface area such as zeolites. The

reciprocal process of adsorption is known as desorption. Gas mixture separation benefits from adsorption due to the varying affinities of gases for a solid adsorbent. This property allows for the selective separation of gas components. The principles of adsorption have been established for over a century, and today the process technology has advanced significantly. This has led to a wide range of applications, including, for example, water treatment, drying, and hydrogen purification. Adsorption is particularly effective at high pressures and low temperatures, which makes it possible to regenerate the adsorbent by reversing these conditions. As a result, pressure swing adsorption (PSA) and temperature swing adsorption (TSA) processes have been developed and widely utilized. When combining multiple adsorber vessels, conducting the different ad- and desorption steps simultaneously, it is possible to continuously separate components of large gas flows in industrial process plants. [20] Thus, a precise step sequence needs to be followed be followed. An exemplary sequence for a four-bed PSA is presented in Figure 2-6. In this particular instance, *Bed A* is utilized for adsorbing the desired species, yielding high-pressure (HP) product with the desired composition. Simultaneously, *Bed B* is purged at a low pressure to promote the desorption process and regenerate the adsorbent. The LP product now contains the previously adsorbed species. *Bed C* and *Bed D* are in intermediate stages. As the beds have differing pressures during this sequence, using intelligent pressure equalization between them can help to lower the power demand of the compressors. For example, the elevated pressure from *Bed C* can be used to partially repressurize *Bed D* and purge *Bed B*. Once *Bed A* is unable to adsorb more impurities, the subsequent step in the sequence is initiated and the beds assume different roles accordingly. [21]

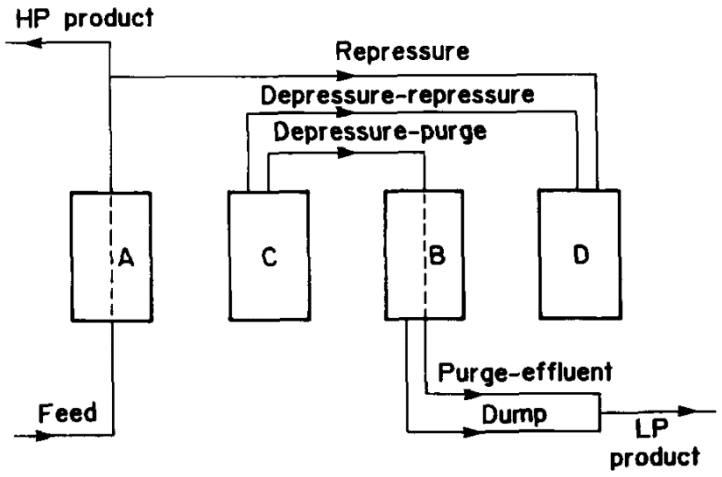

Figure 2-6: Exemplary cycles of a four-bed pressure swing adsorption unit [21]

When it comes to the specific application of separating CO_2, CO and O_2 which are typically the components of the product gas of a CO_2 conversion reactor, zeolites appear to be very promising as absorbents. *Perez-Carbajo et al.* [22] screened various zeolite materials on basis of molecular simulations in combination with ideal adsorption theory. Their study proposes the use of two zeolites in a combination of two PSA units. In the first PSA, CO_2 is separated by means of a FAU zeolite. In the second PSA, it is suggested

to use a BRE zeolite to capture the CO. Both PSA cycle operate at an adsorption pressure of 2 bar and a regeneration pressure of 0.1 bar, utilizing a four-bed process design. More details can be found in the supplementary documentation of reference [22]. A product gas purity of 98,73% CO could be achieved. However, it should be noted that these theoretical results have yet to be reproduced experimentally.

Second, there are membrane-based separation technologies. Gas separation membranes allow one component in a gas stream to pass through faster than the others. The separation mechanism of this pressure driven process is highly dependent on the type of membrane. For very porous membranes typically the Knudsen diffusion and Poiseuille flow are the dominating permeation mechanism. The selectivity for binary gas mixtures can be estimated from the square root of the ratio of the molecular weights. For non-porous membranes the gas transport is usually described as solution-diffusion mechanism. The gases first dissolve in the membrane and then diffuse though it. This enables the ability to control the separation selectivity by adjusting the membrane material according to the properties of the different species. [23] Typical industrial applications of membrane-based gas separation are the production of nitrogen and oxygen enriched gases, H_2 recovery from refinery streams and CO_2 separation from natural gas. Even though the research on gas separation membranes, in particular polymeric membranes, has advanced in the recent years, the growth of large industrial applications is slowed down due to the problems such as membranes lifetime, selectivity, and permeability. Moreover, the achievable degree of separation is comparably low leading to the necessity of multistage separation steps depending on the process requirements. [24]

For the gas separation in the CO_2 conversion process, membranes are a potential alternative for adsorption-based separation technologies. Particularly polyimide membranes *(Matrimid®)* might be promising since decent values of permeability and selectivity for the separation of CO_2 from CO have been achieved in experimental investigations. [25] Furthermore, O_2-conducting ceramic hollow fiber membranes are being considered for use in MW plasma reactors to separate O_2. [26] However, there are currently no (experimental) results available to determine whether their performance is adequate for industrial use.

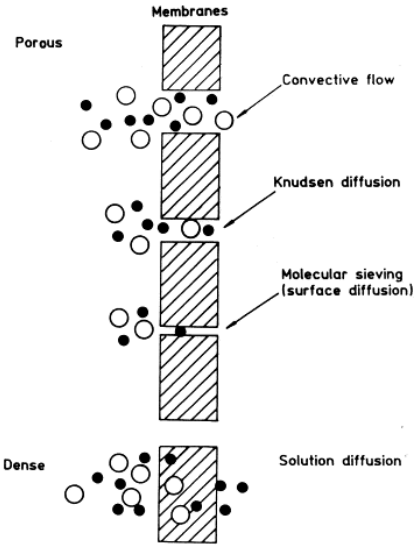

Figure 2-7: Different transport mechanism in membrane-based separation processes [23]

Third, there are electrochemical separation technologies. By means of gas diffusion electrodes (GDE) it is theoretically feasible to effectively separate the oxygen from the product gas. GDE which are usually used in the electrolyzer and fuel cell industry, are multi-layer porous electrodes coated with a catalyst. The O_2 molecules are able to permeate through the GDE, where they are catalytically converted into OH^- and dragged to the anode. Eventually, the recombination reaction occurs and the oxygen can be removed from the system. [27] The basic working principle is illustrated in Figure 2-8. A proof of concept was already provided by *Kaufmann et al.* [27], however, for the industrial application the technology readiness level needs to be further increased.

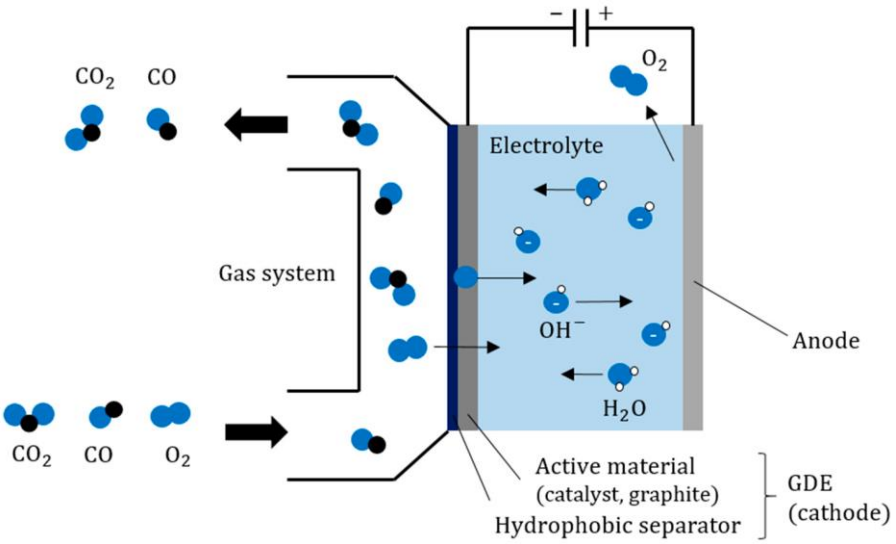

Figure 2-8: Basic working principle of a gas diffusion electrode for oxygen separation [27]

Other gas separation methods, such as absorption or cryogenic separation are widely used in the chemical industry as well. CO_2 absorption with amines and cryogenic distillation are both considered in post-combustion carbon capture from flue gas. However, both technologies tend to have a very high energy demand. [28] Additionally, neither technology has been specifically researched for the application of separating the ternary mixture of CO_2, CO and O_2. Thus, these options are not under consideration for the process design in this work. Another worthwhile alternative to the conventional separation methods is the in-situ trapping of oxygen. By introducing a hydrogen source, such as pure H_2 or CH_4, into the feed gas, the O_2 can be chemically converted to H_2O within the plasma reactor. This method facilitates easier subsequent separation of gas components since H_2O can be separated more easily than O_2. However, this comes at a cost of reduced CO_2 conversion efficiency in the plasma reactor. [29] Since this work solely focusses on the conversion of pure CO_2 as outlined in chapter 3, this concept is not taken into consideration.

3 Methodology

In this chapter the fundamentals and the methodology for the design and simulation of the plasma-based CO_2 conversion process as well as the techno-economic evaluation are outlined. Moreover, the data basis, boundary conditions, simplifications as well as made assumptions are illustrated.

3.1 Process Design and Simulation

In order to achieve a greater understanding on how a large-scale MW plasma-based CO_2 conversion process could look like, a concept for a process for industrial applications is designed. Furthermore, to enable an analysis on how a MW plasma reactor operates in an integrated process, thermodynamic flowsheet simulations are done with the software *Aspen Plus V12*.

The process simulation is based on the research conducted by *Hecimovic et al.* [7], which investigated the performance of a 2.45 GHz microwave plasma torch in a reverse vortex configuration with cooled effluent channels. The experimental data, which has been provided for this work, include the conversion rates χ_{CO2} obtained with the MW plasma reactor at different operating point (pressure, power input, and flow rate). Hence, a case study was conducted using *Aspen Plus* software to determine the optimal operating point for overall process.

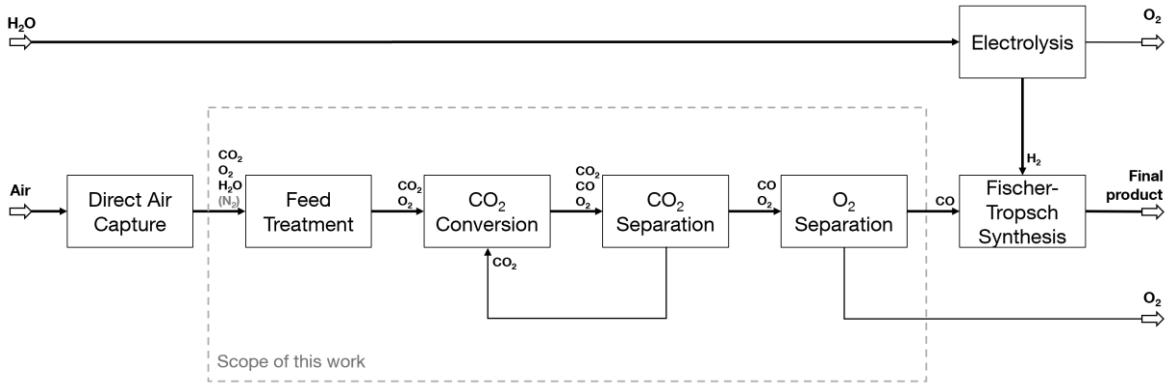

Figure 3-1: Block flow diagram of a basic plasma-based CO_2 conversion process integrated in a possible production path for renewable fuels

For the general design of the process two major process boundaries were determined First, the CO_2 shall be supplied by a direct air capturing (DAC) plant. DAC was chosen over other, significantly cheaper CO_2 sources such as inherent carbon capture in chemical process because it enables the final product to be carbon-neutral. The second process boundary – the downstream process – was determined to be a Fischer-Tropsch plant. In combination with an electrolysis unit that provides green hydrogen, synthetic fuels can be produced through hydrogenation of CO and H_2. [30] Fischer-Tropsch syn-

thesis was chosen over other processes like methanol synthesis due to its advantages operating conditions (e.g. lower operating pressures) and its versatility in producing a various commodity chemicals. [31, 32]

The integration of the plasma-based CO_2 conversion reactor in such a process necessitates additional unit operations to ensure proper operability of all units and the quality of the products. This involves removing impurities from the DAC plant's feed gas and separating the gas mixture leaving the reactor (CO_2, CO, O_2). In Figure 3-1 a basic block flow diagram is given including the up- and downstream process units. Additionally, the scope of this work is indicated. The detailed process flow diagram (PFD) for this part of the process can be found in Appendix A). The design and modelling of the therein included units are described in chapters 3.1.2 and 3.1.3. The main plant parameters such as CO_2 capacity are summarized in Table 3-4 in chapter 3.3.3.

3.1.1 Flowsheet Simulation Setup

After establishing the boundaries, the process simulation is set-up by following a typical procedure which is outlined in the following. A comprehensive introduction to process design and simulation is available in [33].

1. Components selection

   The first step is the selection of all required components. For the case of the CO_2 conversion these are CO_2, CO and O_2 according to equation (2-1). However, since the CO_2 of DAC plants typically includes impurities, these have to be considered in the component selection as well. For the specification of the CO_2 feed stream the data of the process by process by *Carbon Engineering* [34] was used which includes the following impurities: O_2, N_2 and H_2O.

2. Property Methods and Phase Equilibrium

   The second step includes the selection of a suitable property method. This step is crucial since the accuracy and credibility of simulation results are highly dependent on the calculation of the physical properties. The selection of the property method is done based on the components, the process type, and the systems thermodynamics. In this work, the *Peng-Robinson* equation of state was chosen. This cubic equation of state for thermodynamic properties that is commonly used to simulate gas processing plants and is well-suited for the modelling of light gas such as CO_2 (mixtures). Additionally, the method is particularly suitable for high temperature (and high pressure) regions. The model can access a various physical property databanks that are embedded in the simulation software. [33]

3. Process Flow Diagram

   After the selection of the components and the property method the process flow diagram (PFD) is implemented. The PFD includes all equipment and indicates the main process and utility streams. In the case of the design of a new process, as it is done in this work, the PFD is typically derived from simple block diagrams. *Aspen Plus* provides a selection of predefined block models for any kind of equipment and unit operation such as reactors, compressor, vessels etc. Anyhow, the

simulation flow diagram might differ from the real PFD, for example when a real equipment is modelled with multiple unit operation blocks in the software or vice versa.

4. Equipment and Flowsheet Specification

   The final part of the setup of a process simulation is the specification of the equipment and supplementary blocks such as the design specification (DESIGN-SPEC) and calculator blocks (CALC) as well as tear streams and convergence properties.

   DESIGN-SPEC blocks are used to specify desired values for flowsheet variables. Besides the input of the target value, an additional variable must be selected to be adjusted to satisfy the design specification.

   CALC blocks can be used to insert *Fortran* statements or *Excel* spreadsheet calculations into the flowsheet computation. This enables, for example, the calculation dependent input variables or evaluation individual KPI.

   Since the designed process includes a recycle stream whose intensive and extensive properties are defined by the process itself, an iterative calculation is required. In *Aspen Plus*, such streams are defined as *tear streams*. Depending on the character of the *tear stream* different calculation algorithm are proposed by the software. Furthermore, it is possible to adjust convergence tolerances and iterative calculation boundaries for all blocks if necessary. [35]

3.1.2 Feed Treatment and Gas Separation

The feed treatment is specified for the CO_2 stream of the DAC process by *Carbon Engineering* [34], as described earlier. The is feed gas is provided with the following composition, given in percent by weight: 97.12% CO_2, 1.51% N_2, 1.36% O_2 and 0.01% H_2O. [34] The relatively low amount of oxygen is not problematic for the CO_2 conversion process as it is a side product of the conversion reaction. Thus, it is not separated from the feed gas.

Nitrogen contents below 50% barely influence the CO_2 conversion nor the efficiency in plasma-based CO_2 conversion processes and therefor are not a critical impurity from a process engineering point of view. However, the presence of nitrogen will cause the formation of harmful nitrogen oxides such as N_2O or NO_x. [36] In the scope of this thesis, the N_2 impurities in the feed gas are not considered. This is because the regarded process is strictly designed based on experimental data which were obtained without the presence of nitrogen. Thus, no data about the formation of nitrogen oxides is available for this reactor setup making the design of downstream separation step not reasonable. Furthermore, N_2 impurities could be completely avoided by powering the calciner in the DAC process with waste heat and/or electricity instead of methane firing.

The third impurity, water, is very critical for the plasma-based CO_2 conversion process as already small amounts of water cause a significant decrease of the conversion rate, for instance by recombination of CO and OH radicals to CO_2. [4] Hence, the water content in the feed gas must be reduced as far as possible before entering the MW plasma

reactor. This drying step is designed as a TSA on activated alumina based on literature data [37, 38]. The implementation in *Aspen Plus* is done by a simplified modelling of the dynamic TSA in a steady-state simulation environment. Therefore, a separation block (SEP) is added to the flowsheet which receives the spilt factors for the separation by a calculation block. It is assumed, that 100% of the water is separated, however, due to the competitive adsorption of CO_2 and H_2O at low humidities, the drying step also comes with CO_2 losses. [37] The split factor for the CO_2 is calculated based on the adsorption isotherms of the binary mixture of CO_2 and H_2O presented in [37].

The product gas separation, is implemented with two PSA units based on the data by *Perez-Carbajo et al.* [22] presented in chapter 2.3. The adsorption-based separation was chosen over to other technologies due to its high technology readiness level and the already commercially available absorbent material. Similarly to the TSA, both PSA units are integrated in the steady-state process by means of separation and calculator blocks. In the first PSA, the CO_2 is adsorbed. Consequently, after being desorbed and recompressed it is recycled to the reactor. As in the work of [22], it is assumed that the purified gas does not contain any CO_2. Thus 100% of the non-converted CO_2 is separated. In the second PSA the CO is adsorbed to be separated from the O_2. The O_2 content in the product gas should not exceed a concentration of 1-2% to be properly processed by the downstream Fischer-Tropsch plant without causing thermal issues. [27, 39] For the pressurization of the PSA units as well as for the recycle, isentropic compressors are used. A mechanical efficiency of 99% and an isentropic efficiency of 89% is assumed for all compressors.

3.1.3 CO_2 Conversion

The design and implementation of the MW plasma reactor is based on experimental data by Hecimovic et al. [7] as described earlier. Therefore, the *Aspen Plus* reactor model *RStoic* is used, since it not only allows inputs for power, temperature, or pressure but also the definition of reaction equations, the conversion rate, and the heat of the reaction. *RStoic* is a stochiometric reactor model that computes the product properties by means of the reaction equations and the defined conversion rate without the specification of the reaction kinetics. [35] The reactor is modelled in a black box approach, which means that it is tuned to fit the experimental data but not necessarily considers all occurring reactions and physical phenomena (refer to Figure 3-2). Moreover, it not only represents the conversion step itself, but also the fast gas quenching, which is necessary to inhibit possible back reactions. To achieve this, a notational heat of reaction is defined. Its value is adjusted by a *DESIGN-SPEC* in order to receive a target outlet temperature of $T_{Out} = 800°C$. The notional heat of reaction includes the energy required for the conversion of CO_2 according to equation (2-1) as well as all the energy, which is lost in different components of the reactor, for instance the gas quench, the losses of the MW source, and other heat dissipations. This workaround enables integration of the experimentally measured wall-plug power demand of the MW reactor in *Aspen Plus,* while simultaneously receiving the correct results for the gas composition and physical properties at the reactor outlet.

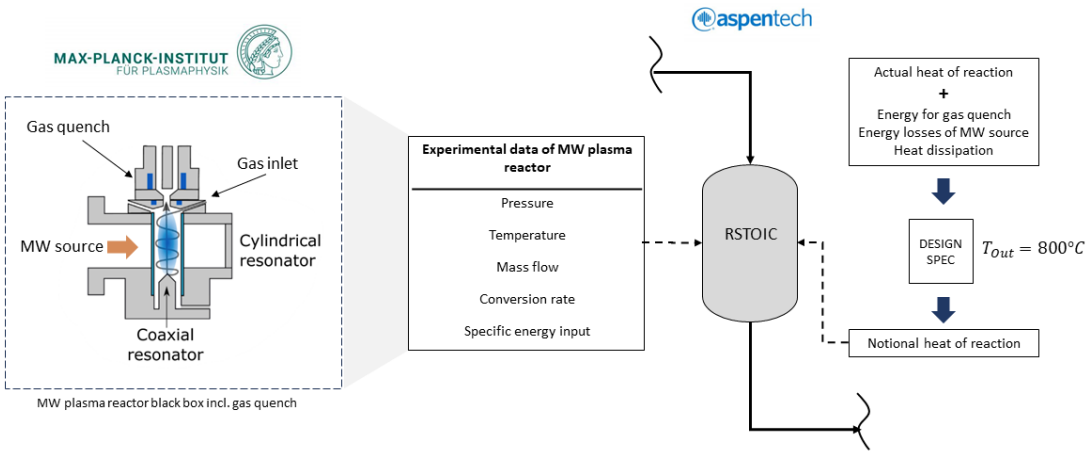

Figure 3-2: Methodology of the experimental data implementation into the RStoic reactor model in Aspen Plus

To achieve the same CO_2 molar flow rates at the reactor inlet as in the experimental setup, despite the presence of a recycle stream, an additional *DESIGN-SPEC* was implemented. This *DESIGN-SPEC* ensures that the sum of the feed gas and recycle gas equals the desired molar CO_2 flow at the reactor by adjusting feed gas flow rate.

The pressure for the CO_2 conversion was set at 1.00 bar(a), despite the experimental data were obtained at slightly reduced pressures in the range of 0.870 to 0.987 bar(a). This is because studies have indicated that nearly identical outcomes can be attained at atmospheric pressure, which not only simplifies the process but also reduces costs. [7] As a result, the vacuum pump can be omitted in the simulation.

3.2 Technological Evaluation

The technical evaluation aims to gain deeper insights into the operation of a MW plasma reactor as a component within a larger process. It also involves analyzing how individual process units affect the overall system's performance and efficiency. To facilitate this assessment, a set of key performance indicators (KPI) is calculated, which not only evaluate the process but also allow for comparisons with similar technologies.

The main technological KPI is the total efficiency η_{Total} of the process as defined in equation (3-1). Where the product in the numerator equals the chemically bound energy in the CO product stream and $P_{E,\mathrm{Total}}$ stands for the total electric power consumption of the process. $P_{E,\mathrm{Total}}$ is calculated as the sum of the power consumption P_E^i of the individual equipment such as the MW plasma reactor or the compressors (refer to equation (3-2)). Here, n is the total number of electrically powered equipment.

$$\eta_{\mathrm{Total}} = \frac{LHV_{CO} * \dot{n}_{CO}}{P_{E,\mathrm{Total}}} = \frac{\Delta H_R * \dot{n}_{CO}}{P_{E,\mathrm{Total}}} \tag{3-1}$$

$$P_{E,Total} = \sum_i^n P_E^i \tag{3-2}$$

Furthermore, the plasma efficiency as defined in equation (2-2) is used for the comparison of the process performance with the stand-alone plasma reactor. For the evaluation of utilization and losses of the CO_2 within the process, a carbon efficiency η_{Carbon} is calculated according to equation (3-3). Where $\dot{n}_{\mathrm{CO2,Feed}}$ is the molar flow of CO_2, that is introduced to the system with through the feed stream and $\dot{n}_{\mathrm{CO,Product}}$ is the useful molar flow of CO that leaves the system through the compressed product gas stream.

$$\eta_{\mathrm{Carbon}} = \frac{\dot{n}_{\mathrm{CO,Product}}}{\dot{n}_{\mathrm{CO_2,Feed}}} \tag{3-3}$$

In the scope of this work two different technological evaluations are conducted. On the one side, the different data points from *Hecimovic et al.* [7] are implemented with a fixed MW source efficiency of 70% assuming that the system is specifically designed for each operation point. This scenario is defined as *Case A*. On the other side, a second evaluation is done where the MW source efficiency is defined as a function of its operating power. Since the experimental setup of *Hecimovic et al.* included a MW source with a nominal power of 3 kW, it can only be operated with a high efficiency when the actual operating power is near the nominal power as shown in Figure 3-3. [40] This evaluation shall give more insights on how the part load operation affects the performance of the whole system. This scenario is defined as *Case B*. The efficiency of the other electrically powered equipment is kept constant in both *Case A* and *B*, since there are no significant influences on the process efficiency by these as presented in chapter 4.1.

The MW source efficiency is defined according to equation (3-5). Where P_{In} is the injected power in form of microwaves and $P_{\mathrm{MW\ Source}}$ the actual power demand of the MW source. This power demand corresponds to the power demand of the MW plasma reactor unit.

$$\eta_{\mathrm{MW\ Source}} = \frac{\mathrm{P}_{In}}{P_{\mathrm{MW\ Source}}} \tag{3-4}$$

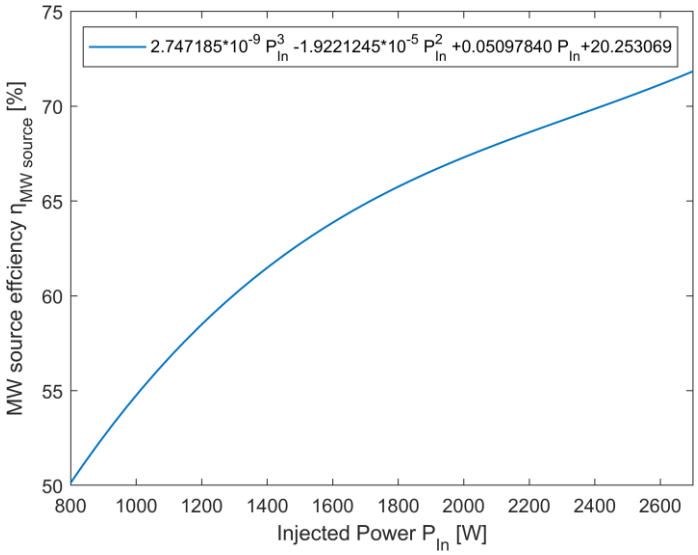

Figure 3-3: Efficiency of a MW source with a nominal power of 3 kW as a function of the operating power [40]

3.3 Economic Evaluation

The economic evaluation aims to calculate the levelized cost of product (LCOP), specifically in this case, the levelized costs of CO. Therefore, all expenses which are associated with the production process must be considered. It can be distinguished between capital expenditures (CAPEX) and operational expenditures (OPEX) which are illustrated in the following. The evaluation is based on methods proposed by *Peters et al.* [41] and *Turton* [42], however, due to the characteristics of the plasma-based process some adjustments are made.

Basis of the economic evaluation is the case study and technological analysis described in the previous chapter. The most promising operation point is selected to be scaled-up to the size of an industrial plant according to the boundary conditions outlined in chapter 3.3.3.

3.3.1 Capital Expenditures

In general, the estimation of CAPEX can be classified in five categories depending on the targeted level of accuracy as shown in Figure 3-4. *Class 1* estimates are the most detailed ones and thus require the highest level of project definition as well as preparation effort. A complete detail engineering of the plant and all utility systems must be conducted. This includes, for example, all major engineering documents such as process and instrumentation diagrams, general arrangement drawings and plot plans. The costs are then estimated based vendor quotes for all expensive items. On the other site of the spectrum, there are *Class 5* estimates, which can be conducted with lower level of project definition and remarkable less effort in order to attain an order of magnitude of the expected costs. Anyhow, these estimates come along with an high uncertainty. [42, 43]

Since the CAPEX evaluation which is conducted in this work is based on a process simulation on PFD-level and includes several estimates due to the special plant characteristics, it can be categorized as *Class 4* or rather *Class 5* estimate.

	Primary Characteristic	*Secondary Characteristic*			
ESTIMATE CLASS	**LEVEL OF PROJECT DEFINITION** Expressed as % of complete definition	**END USAGE** Typical purpose of estimate	**METHODOLOGY** Typical estimating method	**EXPECTED ACCURACY RANGE** Typical +/- range relative to best index of 1 [a]	**PREPARATION EFFORT** Typical degree of effort relative to least cost index of 1 [b]
Class 5	0% to 2%	Screening or Feasibility	Stochastic or Judgment	4 to 20	1
Class 4	1% to 15%	Concept Study or Feasibility	Primarily Stochastic	3 to 12	2 to 4
Class 3	10% to 40%	Budget, Authorization, or Control	Mixed, but Primarily Stochastic	2 to 6	3 to 10
Class 2	30% to 70%	Control or Bid/ Tender	Primarily Deterministic	1 to 3	5 to 20
Class 1	50% to 100%	Check Estimate or Bid/Tender	Deterministic	1	10 to 100

Notes: [a] If the range index value of "1" represents +10/-5%, then an index value of 10 represents +100/-50%.
[b] If the cost index value of "1" represents 0.005% of project costs, then an index value of 100 represents 0.5%.

Figure 3-4: Generic cost estimate matrix [43]

CAPEX include both, the capital required to buy the equipment also known as fixed-capital investment (FCI) and the capital required to operate the plant which is termed working capital (WC). The FCI can be further divided into fixed-capital investment which is directly related to the manufacturing process (direct costs) and nonmanufacturing fixed-capital investment (indirect costs). Assuming that the WC account for 10% of CAPEX [27], they can be calculated as shown in equation (3-5).

$$CAPEX = FCI + WC = \frac{FCI}{0.9} \tag{3-5}$$

The basis of the FCI calculation are the purchased equipment costs. These are taken from the literature (refer to chapter 3.3.3) and if necessary, scaled up to the required capacity by means of equation (3-6).

$$\frac{C_A}{C_B} = \left(\frac{S_A}{S_B}\right)^r \tag{3-6}$$

Here, C stands for the equipment costs and S for the capacity or scale. The exponent r is an equipment-specific value which can be found in the literature, for instance, in [41] and [44].

In order to consider changes in the economic conditions and rising level of prices due to inflation, the purchased equipment costs, which were determined by data from the past must be adjusted to the today's conditions according to equation (3-7). This is done with so-called cost indexes. One cost index which is commonly used in the chemical industry is the *Chemical Engineering Plant Cost Index* (CEPCI). The indices 1 and 2 stand for different points in time. Historical data for the CEPCI can be found in various sources, including [42]. As of the current year, the CEPCI value is 601.3. [27]

$$\frac{C_1}{C_2} = \frac{CEPCI_1}{CEPCI_2} \tag{3-7}$$

After consolidating the total purchased equipment costs (TPEC), there are different methods to derive the FCI. A method often used for *Class 5* estimates is the application of so-called *Lang factors*. The FCI are approximated by multiplying the delivered-equipment costs with a factor that depends on the type of the process plant and includes all direct and indict costs for the plant erection. For fluid processing plant, for example, the TCI would be equal to five times the delivered-equipment costs as shown in Table 3-1. [41]

Table 3-1: Lang factors for the estimation of the fixed-capital investment [41]

Type of plant	Factor to be multiplied by delivered equipment costs
Solid	4.0
Solid-fluid	4.3
Fluid	5.0

The method applied in this work is strongly related to the original *Lang factor* method but allows a better understanding of how the TCI compound. Instead of applying one factor for the estimation of the total FCI, the calculation is broken down to the single cost items. For each cost item, which is a part of the FCI (refer to Table 3-2) a specific *Lang factor* is applied. Afterwards, the sum of all items is calculated (refer to equation (3-8). [41]

Table 3-2: Lang factors for direct and indirect costs for fluid processing plants [41]

	Cost item		Factor
Direct costs	Equipment installation	f_1	0.47
	Instrumentation and controls (installed)	f_2	0.36
	Piping (installed)	f_3	0.68
	Electrical systems (installed)	f_4	0.11
	Buildings (including services)	f_5	0.18
	Yard improvements	f_6	0.10
	Service facilities (installed)	f_7	0.70
Indirect costs	Engineering and supervision	f_8	0.33
	Constructions expenses	f_9	0.41
	Legal expenses	f_{10}	0.04
	Contractor's fee	f_{11}	0.22
	Contingency	f_{12}	0.44

Usually, the provided factors are multiplied with the total delivered-equipment costs. However, in this thesis, this approach is adjusted due to the extremely high TPEC resulting from the expenses incurred in the MW plasma reactor. In order to prevent significant impact on other capital costs, the basis to which the factors are applied was changed to TPEC'. The TPEC' include the costs of all equipment but only take 10% of the costs for the MW plasma reactor into account. Equation (3-8) shows the adjusted method for calculating the FCI. The delivery of the equipment is assumed to be 10% of TPEC' and considered with the factor f_d.

$$FCI = \ TPEC + TPEC' * (1 + f_d) * \left(1 + \sum_{i=1}^{12} f_i\right) \tag{3-8}$$

3.3.2 Operational Expenditures and Total Product Costs

The calculation of total product costs (TPC) considers all expenses associated with the production process. TPC are determined by adding the manufacturing costs and general expenses such as research and development. [41] The manufacturing costs include both OPEX and CAPEX. The latter are included in the form of annualized capital costs (ACC) as illustrated in Table 3-3.

$$TPC = Manufacturing\ Costs + General\ Expenses \tag{3-9}$$

Table 3-3: Typical factors for the calculation of the total product costs [41]

		Cost item	Typical factor	Basis
Manufacturing costs	Variable costs	Raw materials and utilities	Equation (3-10)	
		Operating labor (OL)	Equation (3-11)	
		Operating supervision (OS)	0.15	OL
		Maintenance and repairs (M&R)	0.02	TPEC
		Operating supplies	0.15	M&R
		Laboratory charges	0.10	OL
	Fixed charges	Annual capital costs (ACC)	Equation (3-13)	
		Taxes and insurance	0.02	FCI
		Plant overhead costs	0.60	OL+OS+M&R
General expenses		Administrative costs	0.25	OL
		Distribution and marketing	0.02	TPC
		Research and development	0.05	TPC

The costs for raw materials and utilities C_{RES} are calculated by multiplying the specific costs c_i with the actual demand d_i as stated in equation (3-10). For the regarded CO_2 conversion process, the individual raw materials, and utilities i are electricity, cooling water and CO_2.

$$C_{RES} = \sum_i c_i * d_i \tag{3-10}$$

The operating labor (OL) is calculated as shown in equation (3-11) which is adapted from [42], where N_{OL} is the number of operators required per shift and c_{OL} the specific operating labor costs. Additionally, a factor is added in order to enable the calculation for part load scenarios.

$$OL = 4.5 * N_{OL} * 1960 \left[\frac{h}{operator*a}\right] * c_{OL} * \frac{t_{OP}}{8760 \left[\frac{h}{a}\right]} \tag{3-11}$$

The number of operators N_{OL} required per shift is estimated on basis of the process steps or rather the number of equipment $N_{Equipment}$ as shown in equation (3-12). [42]

$$N_{OL} = \sqrt{6{,}29 + 0{,}23 * N_{Equipment}} \tag{3-12}$$

CAPEX are considered in form of annualized capital costs (ACC). ACC are calculated by multiplying the FCI with the annuity factor (ANF) and adding the interests for the WC (refer to equation (3-13)) as proposed by [45]. The product $ANF * FCI$ is known as an annuity which includes the full capital value of the plant and the interests over the total plant lifetime broken down into constant annual payments.

$$ACC = ANF * FCI + i * WC \tag{3-13}$$

The annuity factor (ANF) is calculated as shown in equation (3-14). Where i is the interest rate and t is the plant lifetime in years.

$$ANF = \frac{i * (1+i)^t}{(1+i)^t - 1} \tag{3-14}$$

The LCOP are derived from the levelized costs of electricity (LCOE) which is a frequently used KPI to assess the economic viability of power plants. Equation (3-15) shows the general definition of the LCOE.

$$LCOE = \frac{Total\ life\ cycle\ costs}{Total\ lifetime\ energy\ production} \cong LCOP \tag{3-15}$$

When calculating the LCOP for the production of CO, the total life cycle costs are not related to the energy production but to the CO mass flow. However, it must be paid attention when comparing LCOP of different sources since there are various ways of calculation. The most frequently calculation methods are either based on the net present value (NPV) [46–48] or based on the annuity method [45, 48–50]. In this work the latter method is applied which can be written as shown in equation (3-16), with the simplification that the amount of CO produced annually and the annual operating costs are constant over the plant lifetime.

$$LCOP = \frac{TPC}{\dot{m}_{CO} * t_{op}} \tag{3-16}$$

3.3.3 Boundary Conditions

In the following, the boundary conditions for the process simulation and the techno-economic evaluation are presented. Table 3-4 shows the main plant parameters which are used for the base case of the techno-economic evaluation. The plant capacity and the costs of CO_2 are adapted from the DAC plant of *Carbon Engineering*. Typical values from the literature are used for the plant lifetime, the interest rate, and the specific costs for labor and cooling water. The annual operating time and the specific electricity costs are based on own assumptions for the base case. However, the influence of the electricity price and the operating time on the LCOP is discussed in detail in chapter 4.3.

Table 3-4: Main plant parameters for the techno-economic evaluation

Parameter	Value	Reference
Capacity (Feed)	171 t/h	[34]
Plant lifetime	25 a	[41]
Operating time	7000 h/a	own assumption
Interest rate	7%	[41]
Labor costs	40 €/h	[51]
CO_2 costs (DAC)	150 €/t	[34]
Electricity costs	0.20 €/kWh	[52] , own assumption
Cooling water costs	0.004 €/t	[27]

Table 3-5 shows the cost functions used to calculate the purchased equipment costs of the main equipment. The specific costs for the MW plasma reactor includes the costs of the main elements that enable the operation of a 100 kW plasma reactor at 915 MHz. [3] The cost for the turbine-generator set is estimated by multiplying the specific cost of the turbine by a factor of 1.8 for heat-recovery steam generators (HRSG) according to [53].

Table 3-5: Cost functions for purchased equipment costs of main process

Component	Cost function			Range of validity	CEPCI	Reference
MW plasma reactor	1400 €/kW			100 kW	2023	[3]
Turbine-Generator set (incl. HRSG)	392 $/kW * 1.8			15000 kW	2016	[53, 54]
	K_1	K_2	K_3	S		
Compressor	2.2897	1.3604	-0.1027	450 – 3000 kW	2001	[42]
Process vessel	3.4974	0.4085	0.1074	0.3 – 520 m³	2001	[42]
Heat exchanger	4.1884	-0.2503	0.1974	10 – 1000 m²	2001	[42]

The remaining equipment costs are estimated by applying the cost function shown in equation (3-17) as proposed by [42]. Where C is the equipment cost for the corresponding capacity or size S. The range of validity as well as the data for K_1, K_2 and K_3 are given in Table 3-5. Due to the high design capacity of the process plant, the range of validity may not be sufficient for all equipment. Therefore, to match the required size or power, the equipment costs are scaled up using equation (3-7) if necessary. For compressors, the capacity parameter S is the power demand, for the process vessels it's the volume and for heat exchangers the heat transfer surface.

$$log_{10}(C) = K_1 + K_2 log_{10}(S) + K_3 [log_{10}(S)]^2 \quad (3\text{-}17)$$

The actual size of each equipment and the quantity required can be found in Appendix E). MW sources (at 915 MHz) are currently only available with a maximum power output of 100 kW. Therefore, the necessary power for the large-scale process, which is analyzed in chapters 4.2 and 4.3, is attained through numbering up rather than scaling up. This also affects the CAPEX calculation as no economy of scale is factored in for the equipment costs of the MW plasma reactor.

4 Results and Discussion

In this chapter the results of the techno-economic analysis of the plasma-assisted CO_2 conversion process are presented and discussed. First, the results of the process simulation and the technological KPI are outlined in chapter 4.1. Second, the economic KPI of an industrial-scale process are evaluated in chapter 4.2. Furthermore, in chapter 4.3, a sensitivity analysis is conducted including the evaluation of different scenarios for operating time and electricity costs.

4.1 Technological Evaluation

The technological evaluation includes the analysis of several operating points for two different cases, as described in chapter 3.1. One evaluation *(Case A)* for a fixed and one *(Case B)* for a variable MW power efficiency. In Table 4-1 the results of the process simulation are summarized for one exemplary operating point of the data set of *Case A*.

The results given in Table 4-1 were obtained at a molar flow of 6.93 mmol/s, a SEI of 238.2 kJ/mol which equals an injected MW power of about 1650 W and a conversion rate of 21.99%. The stream names correspond to the *Aspen Plus* simulation flowsheet which can be found in Appendix A).

A considerably large recycle stream can be observed as a result of the relatively low conversion rate. Furthermore, two carbon losses within the process can be identified. Firstly, a small amount of CO_2 is lost in the dryer step due to the competitive adsorption of H_2O and CO_2 as described in chapter 3.1.2. In total 0.000755 mmol/s of CO_2. The second carbon loss occurs during the separation of CO and O_2. A total of 0.0299 mmol/s CO are included in the waste gas of the second PSA unit (the O_2 product stream). This results in a total carbon efficiency of $\eta_{\mathrm{Carbon}} = 97.99\%$. Due to the comparable feed composition across all operating points and the assumption that 100% of CO_2 can be effectively separated in the first PSA unit (refer to chapter 3.1.2), the carbon efficiency remains constant for all assessed operating points in *Case A* and *B*. For an actual system, a reduced carbon efficiency is expected due to additional carbon losses in the O_2 product stream caused by imperfect CO_2 adsorption in the first PSA unit.

Table 4-1: Summary of the experimental data input and the flowsheet simulation results for an exemplary operating point

Experimental Data Input		
Molar flow	$\dot{n}_{CO_2,In} = 6.93\,\frac{\mathrm{mmol}}{\mathrm{s}}$	corresponds to the molar CO_2 flow at the reactor inlet
Specific Energy input	$\mathrm{SEI} = 238.2\,\frac{\mathrm{kJ}}{\mathrm{mol}}$	for the MW plasma reactor
Conversion rate	$\chi_{CO_2} = 21.99\,\%$	CO_2 conversion in the reactor

Resulting Stream Data

	Unit	**Feed gas**	**Dry Feed**	**Recycle**	**Reactor inlet**	**Reactor outlet**	**Product O_2**	**Product CO**
Stream name		FEED-G1	DRY-G1	R-GAS-5	REAC-I1	REAC-O1	O2-PROD	CO-PROD
Molar flow	$\frac{\mathrm{mmol}}{\mathrm{s}}$	1.554	1.553	5.51	7.06	7.83	0.801	1.513
Temperature	℃	25	25	25	25	800	45	150
Pressure	bar	1	1	1	1	1	2	2
Molar fraction								
CO_2	-	0.9811	0.9814	0.9810	0.9811	0.6909	0	0
CO	-	0	0	0.0140	0.0109	0.2046	0.0373	0.9873
O_2	-	0.0186	0.0186	0.0050	0.0080	0.1046	0.9627	0.0127
H_2O	-	0.000243	0	0	0	0	0	0

Resulting Electrical Power Consumption

	Unit	**MW plasma reactor**	**Recycle compressor**	**PSA compressors**	**Product compressor**
Power	W	2358.2	96.00	21.27	32.04

For the exemplary operating point in Table 4-1, the overall energy efficiency of the CO_2 conversion system is 16.86%, the highest among all the operating points in *Case A.* In Figure 4-1 the total energy efficiency as a function of the conversion rate in the MW plasma reactor is given for all operating points. In Addition, each series of measurement at a specific molar flow is clustered for easier classification as stated in the diagram legend.

Besides the already evaluated data point, the analysis of *Case A* brought up several other operating points slightly below the maximum, with total efficiencies between 16.74% and 16.82% at conversion rates in the range of 18% to 35% and SEI of 194 to 390 kJ/mol. Generally, the best energy efficiencies were achieved at low to moderate SEI and thus moderate conversion rates. Details about the operating conditions of all evaluated point can be found Appendix C).

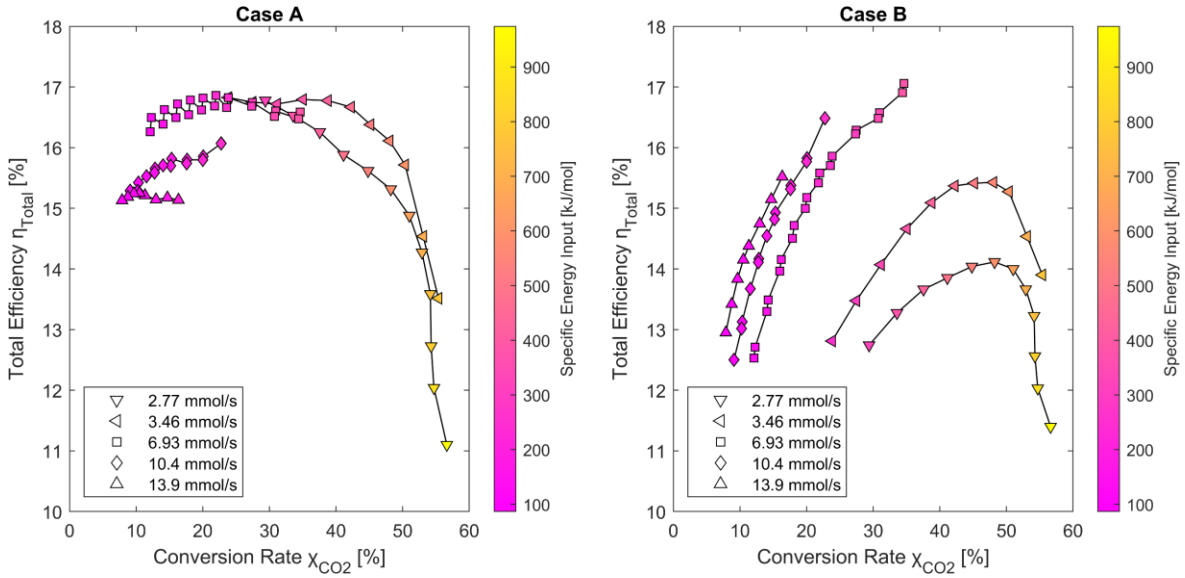

Figure 4-1: Total efficiency for Case A and Case B as a function of conversion rate

When comparing the simulation results of *Case A* with the original experimental data of the MW plasma reactor [7], it becomes obvious that the plasma efficiency has a major impact on the process as a whole (refer to Figure 4-2). The calculated total efficiency of the simulated process appears to have a very high correlation with the plasma efficiency for the most part. Of course, there is a slight off-set due to the additional energy requirements, for example, for the additional separation steps. However, especially at low SEI and thus at low conversion rates the data does not correlate strictly anymore. In the region of $\chi_{CO2} < 21\%$ the total efficiency is decreasing although the plasma energy efficiency continuous to increase. This indicates that another system component has a significant influence on the process efficiency. This behavior is explained more detailed in the section about the evaluation of electricity consumers.

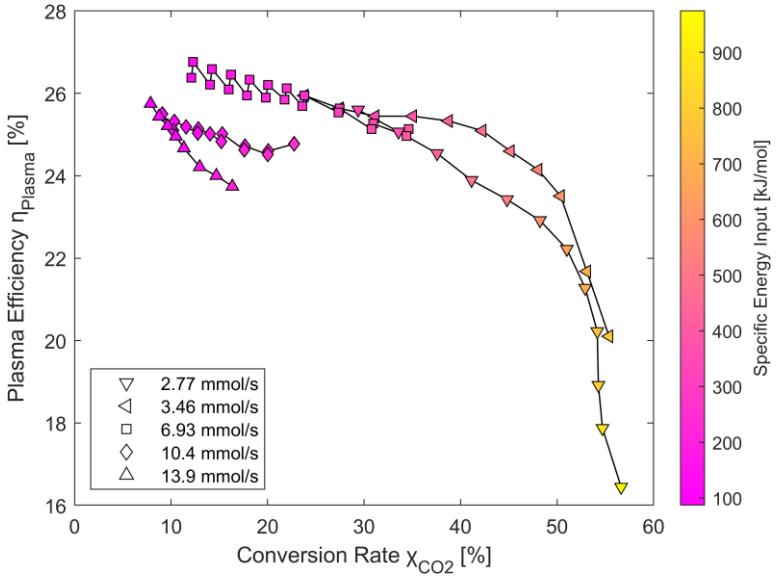

Figure 4-2: Plasma efficiency as a function of conversion rate [7]

Regarding *Case B* it can be seen that the MW source efficiency has a major impact on the overall system performance. When considering the variable MW source efficiency as presented in Figure 3-3, the total efficiency at low operating powers of the MW source decreases significantly. This effect becomes more obvious when comparing the plots of *Case A* and *B* in Figure 4-2. Whilst the total efficiency only slightly decreases at low MW powers (low conversion rates and SEI) in *Case A* there is a steep decrease in *Case B*. For instance, at a molar flow rate of 6.93 mmol/s the MW source efficiency drops from 72.1% (at $\chi_{CO2} = 34.6\%;\ SEI = 389.8\ kJ/mol;\ P_{In} = 2730\ W$) to 52.6% (at $\chi_{CO2} = 12{,}1\%;\ SEI = 129.9\ kJ/mol;\ P_{In} = 900\ W$). At the former operating point, a total efficiency of 17.1% was achieved which is the maximum for *Case B*. A summary of the performance of all operating points in *Case B* is given in Appendix D).

Consequently, when a MW plasma reactor is operated dynamically rather than statically at the rated power, the efficiency of the MW source must always be considered. This also implies that in a large plant where multiple torches are operated simultaneously, partial load cases should be operated not by slightly reducing the power of all torches but shutting down individual torches completely and operating the remaining torches at nominal power. In this way, the total efficiency is not significantly decreased during part load operation.

Figure 4-3 shows the specific electrical power consumption (EPC) (top) and the relative allocation of electricity demand of the main equipment (bottom). The lowest specific EPC which is achieved is 20.80 and 20.56 kWh per Nm³ of CO, for *Case A* and *B* respectively. Both values correspond to operating points with the highest total efficiency presented above. It can be seen that the MW plasma reactor requires by far the most energy. This also explains why the function of the plasma efficiency (refer to Figure 4-2) and the function of total efficiency over the conversion rate (refer to Figure 4-1) show such a high correlation. The deviation at low conversion rates, as mentioned before, can be traced back to the increasing energy demand of the recycle compressor. Since the process is designed to utilize as much CO_2 as possible, the CO_2 which cannot be converted when passing through the reactor is recycled. Thus, the flow rate of the recycle stream is proportional to $(1 - \chi_{CO2})$ leading to high recycle flow at operating points with a low conversion rate. The relative energy demand for the MW plasma reactor accounts for 85.6% at the lowest conversion rate ($\chi_{CO2} = 56.6\%$) and 98.3% at the highest conversion ($\chi_{CO2} = 7.9\%$) rate for *Case A*. The latter operating point also corresponds to the global maximum of the total energy demand as shown in Figure 4-3 (top). The numbers for *Case B* are in the same order of magnitude.

Based on the above technological evaluation, the following recommendations for the operation of a plasma-assisted CO_2 conversion process can be made regarding the energy efficiency. Although the influence of the plasma efficiency on the overall system is significant, the design of the process should not solely focus on achieving the maximum plasma efficiency. In terms of the energy efficiency, a stand-alone MW plasma reactor should be operated at low conversion rates and thus with a high plasma efficiency (refer to Figure 4-2). However, this is not applicable when integrating the reactor into a system with a gas separation unit. A balance between moderate plasma efficiency and higher conversion rates will optimize the overall system performance. This approach minimizes the requirement for the separation and recycling of large amounts of CO_2, which is associated with excessive energy consumption and ultimately results in the greatest total energy efficiency.

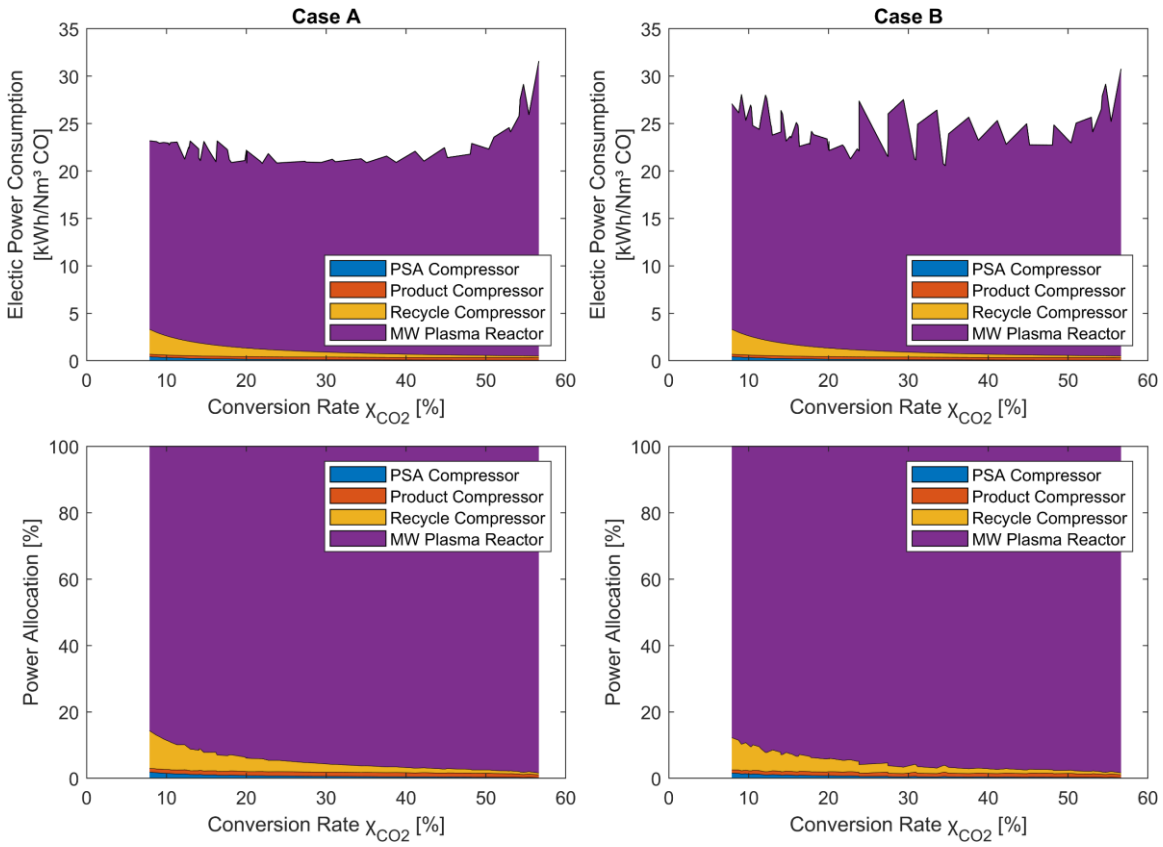

Figure 4-3: Total specific electrical power consumption (top) and total relative electrical power allocation (bottom) of main equipment as a function of conversion rate for Case A (left) and Case B (right)

A remaining issue of the design of this plasma-based process is the heat integration. As a large fraction of the MW power is not directly utilized for the conversion reaction, the gas temperature[2] in the reactor can get very high (~6000K) [7]. Therefore, the lab scale reactor from which the data of this thesis is obtained, has a special design with a gas quench. The gas quench inhibits the recombination of O_2 and CO and is an essential part to achieve a high conversion rate. The gas has to be cooled down to approximately 800°C to achieve this. Since this must happen very fast, the transported heat is not available at an attractive temperature level afterwards with this specific reactor design. Hence, it cannot be used, for example, for steam generation. Only the excess heat in the range from 800°C to about ambient temperature is theoretically useable in this setup.

One theoretically possible use of this heat is to preheat the feed gas for the reactor. However, experimental results about the effect of a preheated feed on the reactor efficiency have not yet been published. Since there is no further demand for high temperature heat within the process itself, the next better option (without exporting waste heat) is

[2] The temperature in the quartz tube is highly inhomogeneous. Thus, the 6000K correspond solely to the reaction zone, where the gas discharge is happening. The bulk temperature is considerably lower.

the production of steam for power generation. The produced electricity can be used, for example, to power plasma reactor.

Also theoretically possible is the integration of the excess heat into one of the up- or downstream processes (refer to Figure 3-1). The Fischer-Tropsch synthesis, however, is a highly exothermic process and even provide excess heat by itself. So there is no reasonable integration of the waste heat from the plasma process. [55] The upstream DAC process, for instance the one by *Carbon Engineering,* seams more promising in terms of heat integration due to the high energy demand of the calciner. The utilization of the waste heat in the methane fired calciner [34] would not only reduce the demand for methane and oxygen but also may decrease the nitrogen impurities in the CO_2 stream. This is because the nitrogen is introduced together with the oxygen from an air separation plant. Thus, if less power must be provided by the combustion of methane, less oxygen and therefore less nitrogen would be introduced into the system.

The electrolysis unit that supplies hydrogen for the Fischer-Tropsch synthesis offers opportunities for heat integration as well. Requirement therefor is the application of a high-temperature electrolysis. Thus a part of the electrical energy can be substituted with thermal energy. [56] The low-temperature fraction of the waste heat can be used to vaporize the water. Thus, the electricity that would be required for the phase change within the electrolyzer can be directly replaced by waste heat. The high-temperature fraction of the waste heat can then be used to further increase the steam temperature, which reduces the electricity demand as well. However, after the phase change more thermal energy must be supplied than electricity is saved. [57]

Other possible applications, of course, would be the integration of the excess heat in another heat demanding process nearby, if the plant is built in a chemical plant complex. In most of the cases, the direct utilization of waste heat by integration in another process is the superior solution compared to the generation of steam for electricity production. However, since this requires detailed process data of the other process, in the following economic evaluation of an industrial-scale plant, the excess is used for electricity production.

4.2 Economical Evaluation

The economic evaluation is based on the most promising operating point of the technological analysis, as described in chapter 3.3. In particular, this is the case that was presented in Table 4-1, with an efficiency of 16.86% at a conversion rate of 21.99% and an SEI of 238.2 kJ/mol. Due to the consideration of the waste heat utilization for steam and electricity generation in the industrial-scale process, the actual total efficiency of the CO_2 conversion process is 17.5% is this evaluation.

At first, the TPEC are evaluated. Figure 4-4 depicts the TPEC allocation of the main process units and equipment. The MW plasma reactor makes up the biggest part of the TPEC with a share of over 96.7% which equals 2305 M€$_{2023}$. Besides from the reactor the waste heat recovery system and the PSA for the CO_2 separation are the second and third biggest cost contributors making up 38.9% (30.8 M€$_{2023}$) and 29.1% (23.1 M€$_{2023}$) of the remaining costs.

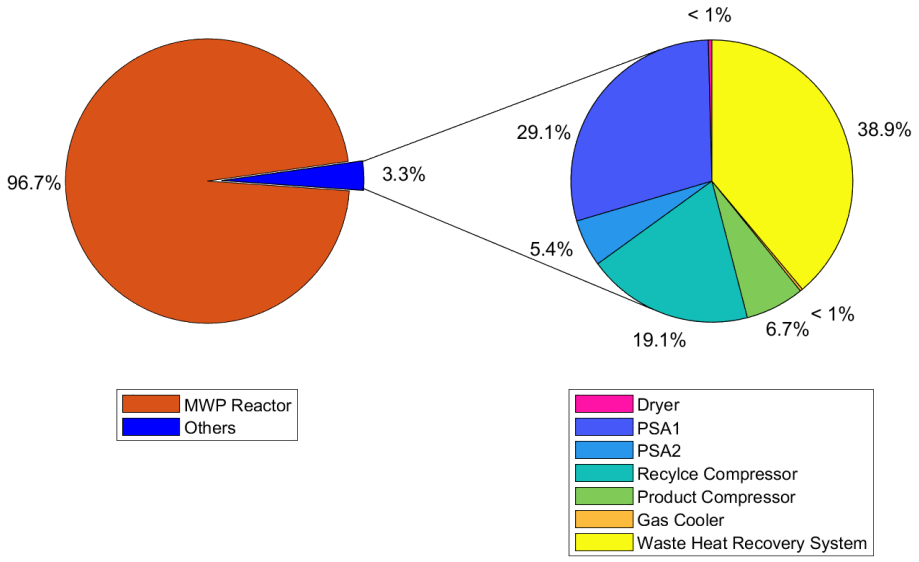

Figure 4-4: Allocation of the total purchased-equipment cost of main process equipment

When applying equation (3-8) this results in FCI of 3378 M€$_{2023}$. With the additional 10% for WC according to equation (3-5) this leads to CAPEX of 3753 M€$_{2023}$. A detailed breakdown of CAPEX is given in Table 4-2. Driven by the costs of the reactor, the delivered equipment makes up the biggest part of the CAPEX with approximately 59%.

Table 4-2: Detailed breakdown of the CAPEX

	Cost item	Costs [M€$_{2023}$]	Percentage of CAPEX
Direct costs	Delivered equipment	2415	59%
	Equipment installation	146	3.6%
	Instrumentation and controls (installed)	111	2.7%
	Piping (installed)	211	5.2%
	Electrical systems (installed)	34	0.8%
	Buildings (including services)	56	1.4%
	Yard improvements	31	0.8%
	Service facilities (installed)	217	5.3%
Indirect costs	Engineering and supervision	102	2.5%
	Constructions expenses	127	3.1%
	Legal expenses	12	0.3%
	Contractor's fee	68	1.7%
	Contingency	136	3.3%
	Working Capital	407	10%
	CAPEX	**4074**	

In Table 4-3 the TPC are broken down to the single cost contributors. The biggest part is the variable cost with approximately 79% mainly driven by the electricity cost which make up for 71% of the TPC. The cost for CO_2 are also not neglectable as they account 5.4% of the TPC. The fixed charges make of 12.2% while in total 10% are ACC. The total overhead contributes 1.2% to the TPC. The above sum up to the manufacturing cost of 93%. The remaining 7% are required for general expenses as described in chapter 3.3.2. In total this results in cost of 3315 M€$_{2023}$ under consideration of the boundary conditions presented in chapter 3.3.3. Considering the CO_2 feed stream of 171 t/h a total of 105 t/h CO can be produced. With the assumed annual operation time of 7000 h, LCOP of 4.44 €/kg$_{CO}$ can be calculated according to equation (3-16). An evaluation of these costs in the context of the current market for bulk chemicals is provided as part of the sensitivity analysis in the following chapter.

Table 4-3: Detailed breakdown of total product costs

		Cost item	Costs [M€$_{2023}$]	Percentage of TPC
Manufacturing costs	Variable costs	CO_2 (DAC)	179	5.4%
		Cooling water	2.1	0.1%
		Electricity	2362	71%
		Operating labor (OL)	17.5	0.5%
		Operating supervision (OS)	2.6	0.1%
		Maintenance and repairs (M&R)	47.7	1.4%
		Operating supplies	7.2	0.2%
		Laboratory charges	2.6	0.1%
	Fixed charges	Annual capital costs (ACC)	343	10%
		Taxes and insurance	73.3	2.2%
		Plant overhead costs	40.7	1.2%
General expenses		Administrative costs	4.4	0.1%
		Distribution and marketing	66.3	2.0%
		Research and development	166	5.0%
		Total Product Costs (TPC)	**3315**	

4.3 Sensitivity and Scenario Analysis

For the evaluation of the impact of different cost parameters a sensitivity analysis is conducted. The considered parameters are the electricity price, the CO_2 price, the operating time per year, and the specific costs for the MW plasma reactor. In Figure 4-5 the LCOP are plotted as a function of the deviation of the above parameters from the base case. The base case values are described in chapter 3.3.3. In addition, detailed sensitivity plots with the specific values of each parameter can be found in the Appendix F).

The electricity price has a significant influence on the LCOP. When operating with 50% cheaper electricity compared to the base case (0.20 €/kWh) the LCOP decrease by almost 40%. The correlation is linear and thus the sensitivity can be written as 0.034 €/%$_{deviation}$. Changes in the price of CO_2 have a much smaller impact on the LCOP than changes in the price of electricity. The gradient equals 0.0026 €/%$_{deviation}$ for the CO_2 price. This means, for instance, that a 50% reduction of the CO_2 price leads to a LCOP reduction of approximately 3%. With a gradient of 0.0065 €/%$_{deviation}$, the specific costs for the MW plasma reactor have a greater influence on the LCOP compared to the CO_2 price but still not as much when compared to the electricity price. Another high sensitivity

occurs when changing the annual operating time of the plant. Since the CAPEX of the plant stay the same when operated at part load, the ACC relative to the CO production increase drastically.

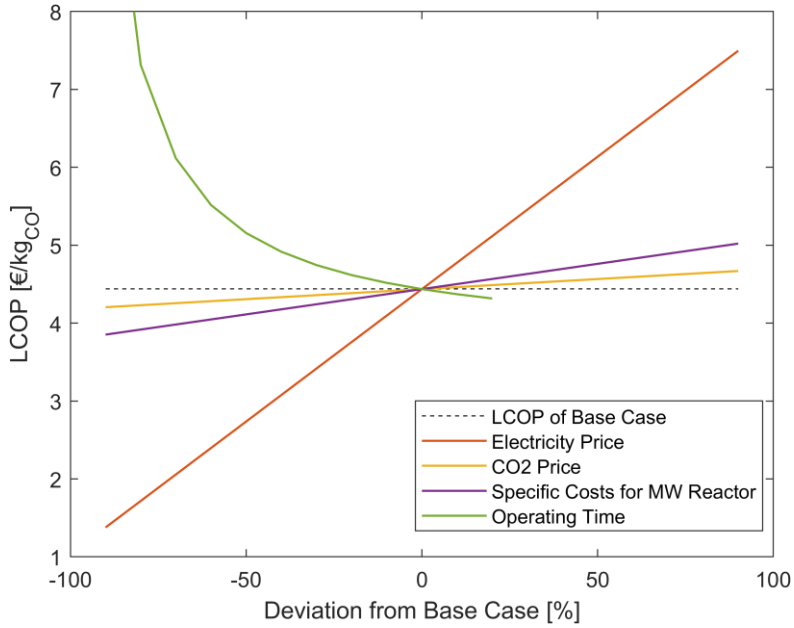

Figure 4-5: Single-variable sensitivity analysis of the LCOP

Of course, the effect of increasing LCOP or LCOE when operating chemical or power plants in part load is well known. Conventional plants are therefore designed to always operate as near as possible at the design capacity. However, especially when it comes to *Power-to-X* (P2X) processes with the aim to produce carbon-neutral chemicals by means of renewable energy, further effects must be considered. The increasing share of renewable energies such as solar and wind in the power sector leads to heavy fluctuations, which may cause a discrepancy between energy production and demand. Since this is highly undesirable, P2X processes are one possible solution for stabilizing the electricity grid or peak shaving. Hence, such systems may not be designed to operate always with the highest load possible but only when excess electricity is produced. This dynamic operation is technically challenging, especially when a process requires, for example, a specific warm-up procedure like a lot of conventional gas-fired reactors have. The plasma-based CO_2 conversion is particularly capable of dynamic operation since the plasma can be easily switched on and off. [17] The main benefit when operating only at energy production peaks is the significantly cheaper electricity price. Anyhow, from an economic perspective this creates and optimization problem for finding the sweet spot of operating at highest load hours with probably higher electricity prices or operating at lower load hours with very low cost for the electricity.

In Figure 4-6 the effect of these dependencies on the LCOP is shown as a function of the operating time. Additionally, the annual load duration curve of the wholesale electricity prices in Germany in 2022 is plotted based on the data of the Bundesnetzagentur [52]. It can be clearly seen that very low operating times are still economically inefficient due to their nonlinear effect on the LCOP. However, the effect of the reduced cost for electricity becomes noticeable and leads to a minimum at about 4000 full load hours per year and 0.13 €/kWh. It is important to note that this is only a simplified illustration, which not

includes several other side effects such as the compensation of ancillary services, economic planning reliability, futures contracts for electricity, the effect of up- and downstream processes and the necessity of gas storages. Even if only a standalone process is considered, dynamic simulations would be required to analyze the system behavior in detail to determine the maximum power gradients for the development of a suitable control concept.

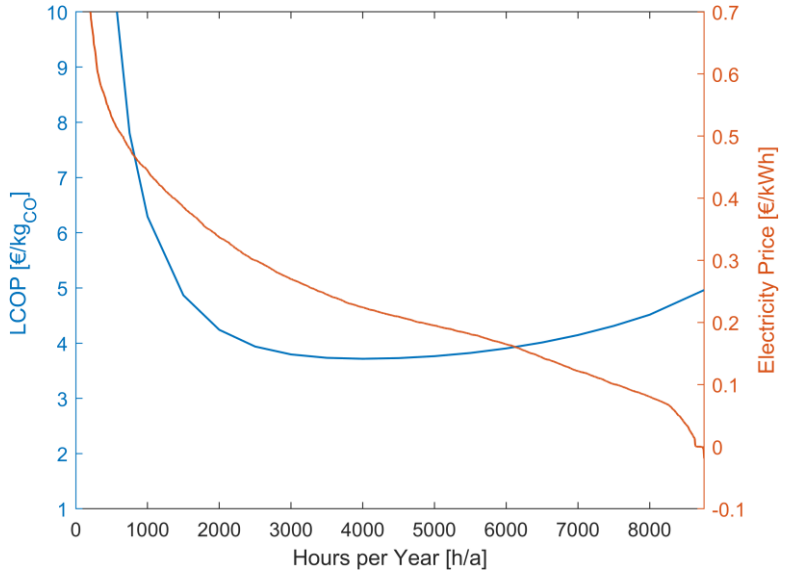

Figure 4-6: LCOP as a function of operating time (left axis) and the annual load duration curve of electricity prices in Germany in 2022 [52] (right axis)

Of course, the process can also run independent from the electricity grid prices when solely powered by renewable energies. For example, when the process plant receives its electricity by a dedicated wind park, that has a nameplate capacity which is equal to the nominal power demand of the CO_2 conversion plant. In this case, when assuming a typical capacity factor of 0.46 (4000 full load hours) [58] and average electricity costs for offshore wind plant of 0.074 €/kWh [59] then the LCOP would between 2.28 and 2.82 €/kg$_{CO}$. The LCOP for several the 'electricity price – load hour combinations' are given in Table 4-4.

Table 4-4: LCOP as a function of the annual operating hours and the electricity price

		Annual full load hours [h/a]									
		500	**1000**	**2000**	**3000**	**4000**	**5000**	**6000**	**7000**	**8000**	**8760**
Electricity price [€/kWh]	**0.031**	10.29	5.55	3.19	2.40	2.00	1.76	1.61	1.49	1.41	1.36
	0.055	10.67	5.93	3.56	2.78	2.38	2.14	1.99	1.87	1.79	1.74
	0.083	11.11	6.37	4.00	3.21	2.82	2.58	2.42	2.31	2.23	2.18
	0.106	11.47	6.74	4.37	3.58	3.19	2.95	2.79	2.68	2.59	2.54
	0.126	11.79	7.06	4.69	3.90	3.50	3.27	3.11	3.00	2.91	2.86
	0.143	12.07	7.34	4.97	4.18	3.78	3.55	3.39	3.28	3.19	3.14
	0.162	12.36	7.62	5.26	4.47	4.07	3.84	3.68	3.57	3.48	3.43
	0.183	12.70	7.96	5.59	4.81	4.41	4.17	4.02	3.90	3.82	3.77
	0.210	13.13	8.39	6.02	5.23	4.84	4.60	4.44	4.33	4.25	4.20
	0.239	13.60	8.86	6.49	5.70	5.31	5.07	4.91	4.80	4.72	4.67

Currently, under the made assumptions, the MW plasma-based CO_2 conversion would not yet be profitable. The market price for CO is approximately 0.65 €/kg according to the *Center on Global Energy Policy at Columbia University* [60].[3] Hence, to see how far the LCOP of CO can be decreased a 'best case' scenario is calculated. Since the lower limit of the different cost parameters can only be estimated in the scope of this work, the result only serves as an indicative value. When assuming very low electricity cost of 0.02 €/kWh, 87 €/t for the CO_2 [34], an annual operating time of 8500 h/a, which equals a availability of 97%, and specific costs for the MW plasma reactor of 850 €/kW (40% decrease compared to current costs), the LCOP could be decreased to 0.93 €/kg_{CO}.

Anyhow, it is important to note that the approximate market price of 0.65 €/kg_{CO} refers to conventional production routes. Due to the higher feedstock costs for air-captured CO_2 and the increased technological complexity of the plasma-based conversion process, well established routes like steam methane reforming for synthesis gas (CO + H_2) production cannot be economically outperformed yet. Nevertheless, the political and economic boundary conditions are evolving. On the one hand, climate policy is going to make production routes with a high carbon footprint increasingly unattractive, for example, by CO_2 emission certificates. And on the other, there is an increasing willingness to pay a premium for carbon-neutral products even in the chemical industry. Particularly, when the final products are sold to industrial customers that have committed to ambiguous decarbonization goals. [61, 62]

As described in chapter 3.3.2, it is difficult to compare LCOP of the plasma-based conversion with competing technologies as there is no standardized methodology for the calculation. Nevertheless, a rough comparison is given in the following for indicative purposes. In a techno-economic evaluation of low-temperature CO_2 electrolysis systems by *Shin et al.* [63] CO production cost of 0.41 €/kg were calculated. This value corresponds to the following boundary conditions: 0.027 €/kWh, 37 €/kg CO_2, 8400 h annual operating time, 20 years plant lifetime.[3] Furthermore, the product costs were calculated by the NPV method instead of the annuity method and cost items like general expenses, taxes and insurances and plant overhead costs have not been considered. [63]

In another evaluation of a low- and high-temperature electrolysis system by *Huang et al.* [64] CO production costs of minimum 1.44 €/kg for the low-temperature process and 0.35 €/kg for the high temperature process are presented. Again, there are some major differences in the methodology since a detailed cash flow analysis was conducted. The details are not explained at this point but can be found in [64]. The assumed electricity price was 0.063 €/kWh and the CO_2 price 37 €/kg.[3]

[3] Original prices are given in USD. The conversion into EUR was made using the following exchange rate: 1.08 $/€. The values were rounded.

5 Summary and Outlook

5.1 Summary

Plasma-assisted conversion processes are considered a viable alternative to conventional techniques for CO_2 conversion. They provide the opportunity for adaptable CO production and can run on renewable energy. By using CO_2 extracted from a DAC plant, the generated CO can be produced in a carbon-neutral way. Coupled with green hydrogen from an electrolysis plant and Fischer-Tropsch synthesis, this enables the production of value-added chemical without CO_2 emissions.

Several institutes are presently developing plasma technologies such as MW, DBD and GA discharges for the efficient conversion of CO_2. In the scope of this work the experimental data gathered from a MW plasma reactor of the *Plasma for Gas conversion* working group of the *Max Planck Institute for Plasma Physics* was used to design a process, which allows the utilization of microwave-based CO_2 conversion in an industrial scale.

The developed process consists of a feed treatment, the CO_2 conversion unit, and a product gas separation unit. In the feed treatment unit, the CO_2 feed gas is dried since already small traces of water decrease the efficiency of the conversion process significantly. In the second step, the dry CO_2 is converted to CO and O_2 in the MW plasma reactor. Subsequently, undissociated CO_2 is separated in a PSA to be recycled to the reactor. A second PSA unit separates the CO and O_2 in order to provide a high purity CO stream. The outlined process design was implemented in the software *Aspen Plus V12*. Both, the feed gas dryer, and the PSA units, have been designed on literature data. Moreover, simplified equipment models were applied to enable the steady-state simulation of these dynamic process units. The reactor was designed on basis of experimental data as outlined before. Consequently, various operating points were analyzed in a case study.

The technological evaluation included the analysis of two different design scenarios. In *Case A*, a fixed MW source efficiency of 70% was assumed for all operating points of the plasma reactor and in *Case B*, the MW source efficiency was implemented as a function of the injected MW power. *Case A* therefore is representative if the system is specifically designed for the single operating point, while *Case B* gives more insights about how the system performs when it is not operated at the rated power but in part load and thus at lower MW source efficiencies. It was shown that the performance of the process as a whole is mainly governed by MW plasma reactor itself. In *Case A*, a high correlation between the plasma efficiency and the total efficiency of the process was shown at medium and high CO_2 conversion rates ($\chi_{CO2} > 21\%$). However, at lower conversion rates, where the plasma efficiency is the highest, the total efficiency was decreased considerably by the increasing power demand for the compression of the recycled CO_2. The highest total efficiency of 16.86% was achieved at a conversion rate of 21.99%. In general, the process is most efficient at medium conversion rates between 20% and 40%, although a

lower plasma efficiency is achieved compared to the low conversion rate cases. This is because less energy is required to compress and recycle the undissociated CO_2 to the reactor. The evaluation of the main electric power consumers has shown that a major part of the electricity demand (between 85.6% and 98.3%) is required by the MW source of the plasma reactor. This also explains the high correlation of the plasma efficiency and the total efficiency of the process.

The evaluation of *Case B* indicates that it is crucial to operate the MW plasma reactor at the rated power of the MW source to avoid decreasing the total efficiency. This must be considered for part load operation of a large-scale process where multiple plasma reactors are operating simultaneously. It is more advantageous to completely shut down individual plasma torches to achieve the required (reduced) power instead of decreasing the power input in all the reactors equally.

In the economic evaluation the most promising operating point of technological evaluation was utilized to calculate the LCOP of a large-scale process plant with a CO_2 feed capacity of approximately 171 t/h. It is noteworthy that the reactor unit not only constitutes the crucial factor for the process performance, but also significantly influences the economics. The plasma reactor accounts for approximately 96.7% of the total equipment costs. However, in this work no economy of scale was considered for the equipment costs of the plasma torches due to the maximum available MW source capacity of 100 kW (at 915 MHz). The necessary total power was achieved by a numbering up. Despite the exorbitant equipment costs, the greatest cost driver for CO production is electricity, as illustrated by the TPC calculation. In the base case, the LCOP aggregates to 4.44 €/kg_{CO}, while the pure electricity costs are around 3.67 €/kg_{CO} at 0.20 €/kWh. For the presented best-case scenario, the lowest achievable LCOP, under the made assumptions, are 0.93 €/kg_{CO}. Additionally, it was demonstrated that LCOPs are highly sensitive to electricity prices and annual operating hours. A dynamic operation can be economically competitive compared to continuous operation at the rated capacity since electricity can be obtained at significantly lower costs, especially when the process runs of renewable energies.

In conclusion, plasma-assisted conversion of CO_2 is a promising technology that can be integrated into a comprehensive process for the industrial production of CO. However, at present the high equipment costs and the high electricity demand due to the moderate efficiency result in comparatively high LCOP. This makes the concept not yet economically attractive when compared, for example, with CO_2 electrolysis.

5.2 Outlook

Since this term paper only offers a first insight into the potential inclusion of a MW plasma reactor in a comprehensive system, further exploration of several aspects is necessary.

In order to decrease the electricity demand, which is the primary driver of the LCOP, enhancing the total energy efficiency of the process is imperative. Therefore, it is crucial to investigate the impact of preheating the feed on conversion performance. This would enable direct utilization of waste heat within the process, if feasible. However, if no positive effects are observed, other heat integration options must be thoroughly analyzed. For instance, integrating all up- and down-stream units in the process simulation could be considered. Anyways, it is equally important to find a solution for utilizing the heat removed through fast gas quenching, as this constitutes the bulk of waste heat and is currently not being utilized.

Furthermore, to facilitate the implementation of MW plasma reactors in industrial processes, it is imperative to conduct a scale-up investigation. Currently, the commercially available MW sources, with a generation frequency of 915 MHz, exhibit a maximum power output of only 100 kW. However, as the maximum power output is higher in MW sources with a lower generation frequency, analyzing the CO_2 conversion at even lower frequencies would provide more insights regarding the upscaling potential. In addition, it is necessary to develop concepts for the integration multiple MW sources into a single reactor unit. The construction of bigger reactors with increased power output has the potential to enable cost savings through economies of scale, particularly for large-scale systems.

Besides the conversion unit, further research is also required for the other process units. Especially, the adsorbents intended to be utilized in the PSA units must be tested experimentally. Moreover, the developments of competing separation technologies must be continuously observed as their technology readiness level increases for the application in the CO_2 conversion process advance.

And finally, as the process design is further refined, it is imperative to conduct dynamic process simulations of the entire system in order to validate the viability of the process utilizing fluctuating renewable energies or for grid stabilization purposes.

References

[1] H. Lee *et al.,* "Climate Change 2023: Synthesis Report: Contribution of Working Groups I, II and III to the Sixth Assessment Report of the Intergovernmental Panel on Climate Change,", IPCC, Geneva, 2023, doi: 10.59327/IPCC/AR6-9789291691647.

[2] IEA, "The Future of Petrochemicals,", IEA, Paris, 2018. Accessed: Sep. 30, 2023. [Online]. Available: https://www.iea.org/reports/the-future-of-petrochemicals

[3] J. F. de La Fuente, A. A. Kiss, M. T. Radoiu, and G. D. Stefanidis, "Microwave plasma emerging technologies for chemical processes,", *J. Chem. Technol. Biotechnol*, vol. 92, no. 10, pp. 2495–2505, 2017, doi: 10.1002/jctb.5205.

[4] R. Snoeckx and A. Bogaerts, "Plasma technology - a novel solution for CO2 conversion?,", *Chemical Society reviews*, vol. 46, no. 19, pp. 5805–5863, 2017, doi: 10.1039/c6cs00066e.

[5] F. A. D'Isa, E. A. D. Carbone, A. Hecimovic, and U. Fantz, "Performance analysis of a 2.45 GHz microwave plasma torch for CO 2 decomposition in gas swirl configuration,", *Plasma Sources Sci. Technol.*, vol. 29, no. 10, p. 105009, 2020, doi: 10.1088/1361-6595/abaa84.

[6] A. Hecimovic, F. A. D'Isa, E. Carbone, and U. Fantz, "Enhancement of CO2 conversion in microwave plasmas using a nozzle in the effluent,", *Journal of CO2 Utilization*, vol. 57, p. 101870, 2022, doi: 10.1016/j.jcou.2021.101870.

[7] A. Hecimovic, C. K. Kiefer, A. Meindl, R. Antunes, and U. Fantz, "Fast gas quenching of microwave plasma effluent for enhanced CO2 conversion,", *Journal of CO2 Utilization*, vol. 71, p. 102473, 2023, doi: 10.1016/j.jcou.2023.102473.

[8] A. A. Fridman, *Plasma chemistry*. Cambridge: Cambridge University Press, 2012.

[9] H. Conrads and M. Schmidt, "Plasma generation and plasma sources,", *Plasma Sources Sci. Technol.*, vol. 9, no. 4, pp. 441–454, 2000, doi: 10.1088/0963-0252/9/4/301.

[10] S. Overa, B. H. Ko, Y. Zhao, and F. Jiao, "Electrochemical Approaches for CO2 Conversion to Chemicals: A Journey toward Practical Applications,", *Accounts of chemical research*, early access. doi: 10.1021/acs.accounts.1c00674.

[11] B. J. Hare, D. Maiti, S. Ramani, A. E. Ramos, V. R. Bhethanabotla, and J. N. Kuhn, "Thermochemical conversion of carbon dioxide by reverse water-gas shift chemical looping using supported perovskite oxides,", *Catalysis Today*, vol. 323, pp. 225–232, 2019, doi: 10.1016/j.cattod.2018.06.002.

[12] O. Hakami, "Thermocatalytic and solar thermochemical carbon dioxide utilization to solar fuels and chemicals: A review,", *Intl J of Energy Research*, vol. 46, no. 14, pp. 19929–19960, 2022, doi: 10.1002/er.8702.
[13] B. Hu, C. Guild, and S. L. Suib, "Thermal, electrochemical, and photochemical conversion of CO2 to fuels and value-added products,", *Journal of CO2 Utilization*, vol. 1, pp. 18–27, 2013, doi: 10.1016/j.jcou.2013.03.004.
[14] R. Gupta, A. Mishra, Y. Thirupathaiah, and A. K. Chandel, "Biochemical conversion of CO2 in fuels and chemicals: status, innovation, and industrial aspects,", *Biomass Conv. Bioref.*, 2022, doi: 10.1007/s13399-022-02552-8.
[15] A. Bogaerts *et al.,* "CO 2 conversion by plasma technology: insights from modeling the plasma chemistry and plasma reactor design,", *Plasma Sources Sci. Technol.*, vol. 26, no. 6, p. 63001, 2017, doi: 10.1088/1361-6595/aa6ada.
[16] A. Bogaerts and R. Snoeckx, "Plasma-Based CO2 Conversion," in *An Economy Based on Carbon Dioxide and Water*, M. Aresta, I. Karimi, and S. Kawi, Eds., Cham: Springer International Publishing, 2019, pp. 287–325.
[17] A. Bogaerts and E. C. Neyts, "Plasma Technology: An Emerging Technology for Energy Storage,", *ACS Energy Lett.*, vol. 3, no. 4, pp. 1013–1027, 2018, doi: 10.1021/ACSENERGYLETT.8B00184.
[18] U. Kogelschatz, "Dielectric-Barrier Discharges: Their History, Discharge Physics, and Industrial Applications,", *Plasma Chemistry and Plasma Processing*, vol. 23, no. 1, pp. 1–46, 2003, doi: 10.1023/A:1022470901385.
[19] S. Gunduz, D. J. Deka, and U. S. Ozkan, "Advances in High-Temperature Electrocatalytic Reduction of CO2 and H2O," in *Advances in Catalysis*, vol. 62, pp. 113–165.
[20] H.-J. Bart and U. von Gemmingen, "Adsorption," in *Ullmann's Encyclopedia of Industrial Chemistry*, Wiley, 2003.
[21] G. G. Haselden, "Gas separation fundamentals,", *Gas Separation & Purification*, vol. 3, no. 4, pp. 209–215, 1989, doi: 10.1016/0950-4214(89)80007-6.
[22] J. Perez-Carbajo *et al.,* "Zeolites for CO2-CO-O2 Separation to Obtain CO2-Neutral Fuels,", *ACS applied materials & interfaces*, early access. doi: 10.1021/acsami.8b04507.
[23] P. Pandey and R. S. Chauhan, "Membranes for gas separation,", *Progress in Polymer Science*, vol. 26, no. 6, pp. 853–893, 2001, doi: 10.1016/S0079-6700(01)00009-0.
[24] P. Bernardo, E. Drioli, and G. Golemme, "Membrane Gas Separation: A Review/State of the Art,", *Ind. Eng. Chem. Res.*, vol. 48, no. 10, pp. 4638–4663, 2009, doi: 10.1021/ie8019032.
[25] R. Checchetto, M. Scarpa, M. G. de Angelis, and M. Minelli, "Mixed gas diffusion and permeation of ternary and quaternary CO2/CO/N2/O2 gas mixtures in Matrimid®, polyetherimide and poly(lactic acid) membranes for CO2/CO separation,", *Journal of Membrane Science*, vol. 659, p. 120768, 2022, doi: 10.1016/j.memsci.2022.120768.

[26] K. Wiegers, A. Schulz, M. Walker, and G. E. M. Tovar, "Determination of the Conversion and Efficiency for CO 2 in an Atmospheric Pressure Microwave Plasma Torch,", *Chemie Ingenieur Technik*, vol. 94, no. 3, pp. 299–308, 2022, doi: 10.1002/cite.202100149.

[27] S. J. Kaufmann *et al.,* "Techno-Economic Potential of Plasma-Based CO2 Splitting in Power-to-Liquid Plants,", *Applied Sciences*, vol. 13, no. 8, p. 4839, 2023, doi: 10.3390/app13084839.

[28] A. Brunetti, F. Scura, G. Barbieri, and E. Drioli, "Membrane technologies for CO2 separation,", *Journal of Membrane Science*, vol. 359, 1-2, pp. 115–125, 2010, doi: 10.1016/j.memsci.2009.11.040.

[29] R. Aerts, R. Snoeckx, and A. Bogaerts, "In-Situ Chemical Trapping of Oxygen in the Splitting of Carbon Dioxide by Plasma,", *Plasma Process Polym*, vol. 11, no. 10, pp. 985–992, 2014, doi: 10.1002/ppap.201400091.

[30] S. J. Davis *et al.,* "Net-zero emissions energy systems,", *Science (New York, N.Y.)*, vol. 360, no. 6396, 2018, doi: 10.1126/science.aas9793.

[31] A. K. Agarwal, A. Gautam, N. Sharma, and A. P. Singh, *Methanol and the Alternate Fuel Economy*. Singapore: Springer Singapore, 2019.

[32] H. Mahmoudi *et al.,* "A review of Fischer Tropsch synthesis process, mechanism, surface chemistry and catalyst formulation,", *Biofuels Engineering*, vol. 2, no. 1, pp. 11–31, 2017, doi: 10.1515/bfuel-2017-0002.

[33] J. Haydary, *Chemical Process Design and Simulation*. Wiley, 2018.

[34] D. W. Keith, G. Holmes, D. St. Angelo, and K. Heidel, "A Process for Capturing CO2 from the Atmosphere,", *Joule*, vol. 2, no. 8, pp. 1573–1594, 2018, doi: 10.1016/j.joule.2018.05.006.

[35] *Aspen Plus V12 Help* (2021). Bedford: Aspen Technology, Inc. Accessed: Oct. 27, 2023. [Online]. Available: https://knowledgecenter.aspentech.com/

[36] R. Snoeckx, S. Heijkers, K. van Wesenbeeck, S. Lenaerts, and A. Bogaerts, "CO2 conversion in a dielectric barrier discharge plasma: N2 in the mix as a helping hand or problematic impurity?,", *Energy Environ. Sci.*, vol. 9, no. 3, pp. 999–1011, 2016, doi: 10.1039/C5EE03304G.

[37] G. Li, P. Xiao, and P. Webley, "Binary adsorption equilibrium of carbon dioxide and water vapor on activated alumina,", *Langmuir : the ACS journal of surfaces and colloids*, vol. 25, no. 18, pp. 10666–10675, 2009, doi: 10.1021/la901107s.

[38] J. Lu, H. Cao, J. Li, and S. Wang, "Heat and mass transfer during H2O/CO2 adsorption separation using activated alumina,", *Heat Mass Transfer*, vol. 58, no. 10, pp. 1771–1783, 2022, doi: 10.1007/s00231-022-03206-1.

[39] A. Herbers, C. Kern, and A. Jess, "Cobalt Catalyzed Fischer-Tropsch Synthesis with O2-Containing Syngas,", *Catalysts*, vol. 13, no. 2, p. 391, 2023, doi: 10.3390/catal13020391.

[40] C. K. Kiefer, R. Antunes, A. Hecimovic, A. Meindl, and U. Fantz, "CO2 dissociation using a microwave plasma torch: A study on industrially relevant pa-

rameters,". [Online]. Available: https://hdl.handle.net/21.11116/0000-000C-F73E-9

[41] M. S. Peters, K. D. Timmerhaus, and R. E. West, *Plant design and economics for chemical engineers,* 5th ed. (McGraw-Hill chemical engineering series). Boston: McGraw-Hill, 2006.

[42] R. Turton, *Analysis, synthesis, and design of chemical processes,* 4th ed. (Prentice Hall international series in the physical and chemical engineering sciences). Upper Saddle River, NJ: Prentice Hall, 2012.

[43] P. Christensen and L. R. Dysert, "COST ESTIMATE CLASSIFICATION SYSTEM: TCM Framework: 7.3 – Cost Estimating and Budgeting,", AACE International, Recommended Practice No. 17R-97, 1997.

[44] D. S. Remer and L. H. Chai, "Process Equipment, Cost Scale-up," in *Encyclopedia of Chemical Processing and Design*, vol. 43, pp. 306–317. [Online]. Available: https://scholarship.claremont.edu/cgi/viewcontent.cgi?article=1794&context=hmc_fac_pub

[45] F. G. Albrecht, D. H. König, N. Baucks, and R.-U. Dietrich, "A standardized methodology for the techno-economic evaluation of alternative fuels – A case study,", *Fuel*, vol. 194, pp. 511–526, 2017, doi: 10.1016/j.fuel.2016.12.003.

[46] IEA, "Projected Costs of Generating Electricity 2020,", Paris, 2020. Accessed: Sep. 6, 2023. [Online]. Available: https://www.iea.org/reports/projected-costs-of-generating-electricity-2020

[47] P. Konstantin, *Praxisbuch Energiewirtschaft*. Berlin, Heidelberg: Springer Berlin Heidelberg, 2013.

[48] G. Allan, M. Gilmartin, P. McGregor, and K. Swales, "Levelised costs of Wave and Tidal energy in the UK: Cost competitiveness and the importance of “banded” Renewables Obligation Certificates,", *Energy Policy*, vol. 39, no. 1, pp. 23–39, 2011, doi: 10.1016/j.enpol.2010.08.029.

[49] S. Tegen, M. Hand, B. Maples, E. Lantz, P. Schwabe, and A. Smith, "2010 Cost of Wind Energy Review,", 2012, doi: 10.2172/1039814.

[50] J. Lehmann, A. Wabbes, E. Miguelañez Gonzalez, and S. Scheerlinck, "Levelized Cost of Hydrogen Calculation from Off-Grid Photovoltaic Plants Using Different Methods,", *Solar RRL*, vol. 6, no. 5, 2022, Art. no. 2100482, doi: 10.1002/solr.202100482.

[51] Statistisches Bundesamt (Destatis), "Labor costs comparison across EU countries per hour worked, 2022,", 2023. Accessed: Oct. 28, 2023. [Online]. Available: https://www.destatis.de/EN/Press/2023/04/PE23_164_624.html

[52] Bundesnetzagentur, "Marktdaten: Großhandelsstrompreise in Deutschland im Jahr 2022,". Accessed: Oct. 8, 2023. [Online]. Available: https://www.smard.de/home/downloadcenter/download-marktdaten/?downloadAttributes=%7B%22selectedCategory%22:3,%22selectedSubCategory%22:8,%22selectedRe-

gion%22:%22DE%22,%22selectedFileType%22:%22CSV%22,%22from%22:1640991600000,%22to%22:1672527599999%7D

[53] F. Cziesla, G. Tsatsaronis, and Z. Gao, "Avoidable thermodynamic inefficiencies and costs in an externally fired combined cycle power plant,", *Energy*, vol. 31, 10-11, pp. 1472–1489, 2006, doi: 10.1016/j.energy.2005.08.001.

[54] U.S. Department of Energy, "Combined Heat and Power Technology Fact Sheet Series: Steam turbines,", 2016. Accessed: Sep. 14, 2023. [Online]. Available: https://www.energy.gov/eere/amo/articles/steam-turbines-doe-chp-technology-fact-sheet-series-fact-sheet-2016

[55] B. Ghorbani, A. Ebrahimi, S. Rooholamini, and M. Ziabasharhagh, "Integrated Fischer-Tropsch synthesis process with hydrogen liquefaction cycle,", *Journal of Cleaner Production*, vol. 283, p. 124592, 2021, doi: 10.1016/j.jclepro.2020.124592.

[56] F. Wang *et al.,* "Thermodynamic analysis of solid oxide electrolyzer integration with engine waste heat recovery for hydrogen production,", *Case Studies in Thermal Engineering*, vol. 27, p. 101240, 2021, doi: 10.1016/j.csite.2021.101240.

[57] L. Mingyi, Y. Bo, X. Jingming, and C. Jing, "Thermodynamic analysis of the efficiency of high-temperature steam electrolysis system for hydrogen production,", *Journal of Power Sources*, vol. 177, no. 2, pp. 493–499, 2008, doi: 10.1016/j.jpowsour.2007.11.019.

[58] IEA, "Average annual capacity factors by technology,", Paris, 2018. Accessed: Oct. 30, 2023. [Online]. Available: https://www.iea.org/data-and-statistics/charts/average-annual-capacity-factors-by-technology-2018

[59] IRENA, "Weighted average levelized cost of electricity for offshore wind worldwide from 2010 to 2022,", 2023. Accessed: 3010.2023. [Online]. Available: https://www.statista.com/statistics/1027721/weighted-average-lcoe-of-offshore-wind-worldwide/

[60] A. Bhardwaj, C. McCormick, and J. Friedmann, "Opportunities and Limits of CO2 Recycling in a Circular Carbon Economy: Techno-economics, Critical Infrastructure Needs, and Policy Priorities,", 2021.

[61] McKinsey & Company, "McKinsey on Chemicals,", 2012. Accessed: Oct. 30, 2023. [Online]. Available: https://www.mckinsey.com/~/media/McKinsey/dotcom/client_service/Chemicals/PDFs/McK_on_Chemicals_The_growing_demand_for_green.ashx

[62] McKinsey & Company, "Sustainable feedstocks: Accelerating recarbonization in chemicals,", 2023. Accessed: Oct. 30, 2023. [Online]. Available: https://www.mckinsey.com/industries/chemicals/our-insights/sustainable-feedstocks-accelerating-recarbonization-in-chemicals

[63] H. Shin, K. U. Hansen, and F. Jiao, "Techno-economic assessment of low-temperature carbon dioxide electrolysis,", *Nat Sustain*, vol. 4, no. 10, pp. 911–919, 2021, doi: 10.1038/s41893-021-00739-x.

[64] Z. Huang, R. G. Grim, J. A. Schaidle, and L. Tao, "The economic outlook for converting CO2 and electrons to molecules,", *Energy Environ. Sci.*, vol. 14, no. 7, pp. 3664–3678, 2021, doi: 10.1039/D0EE03525D.

Appendix

A) Process Flow Diagrams | Aspen Plus Simulation Flowsheet

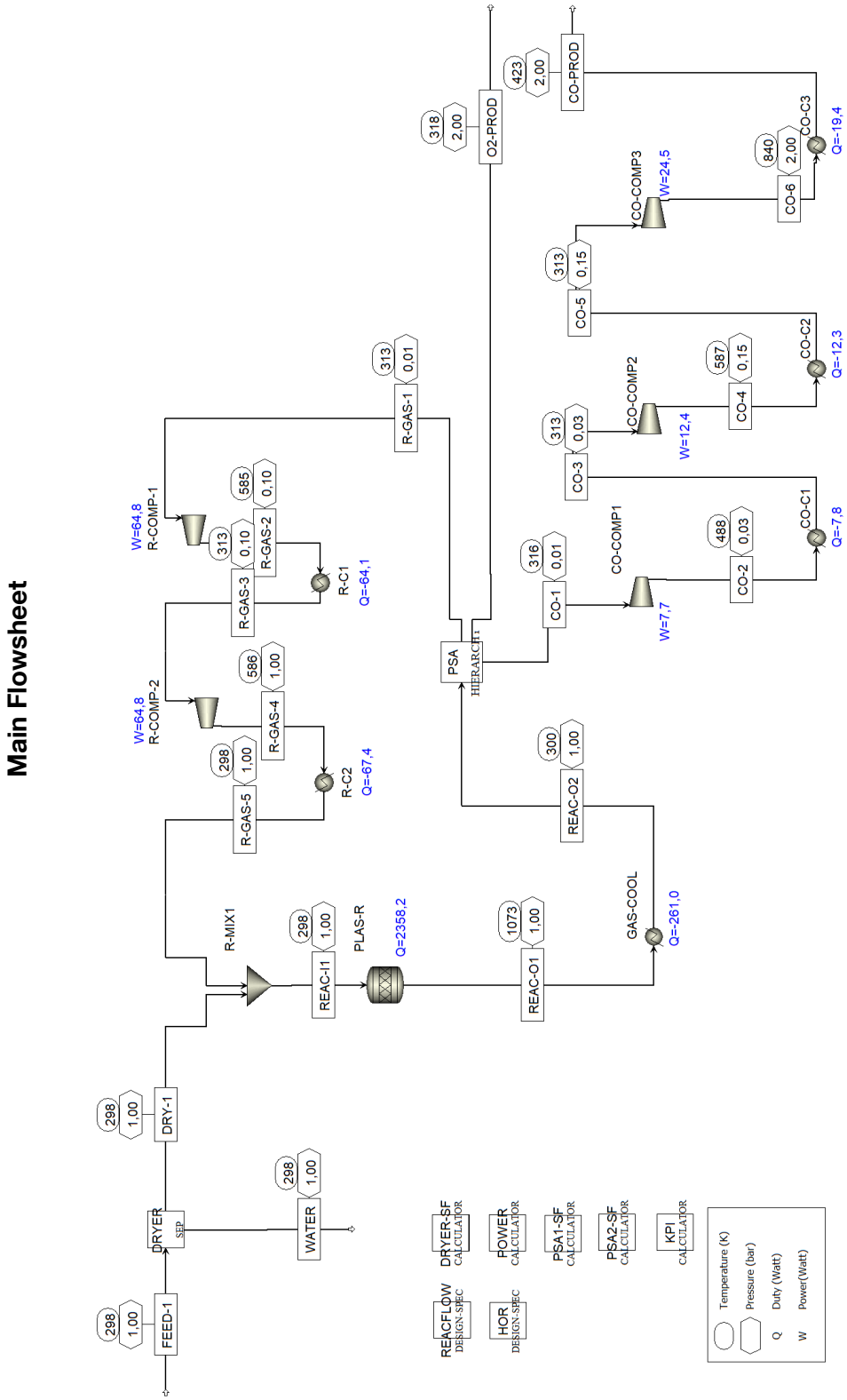

Sub-Flowsheet (PSA)

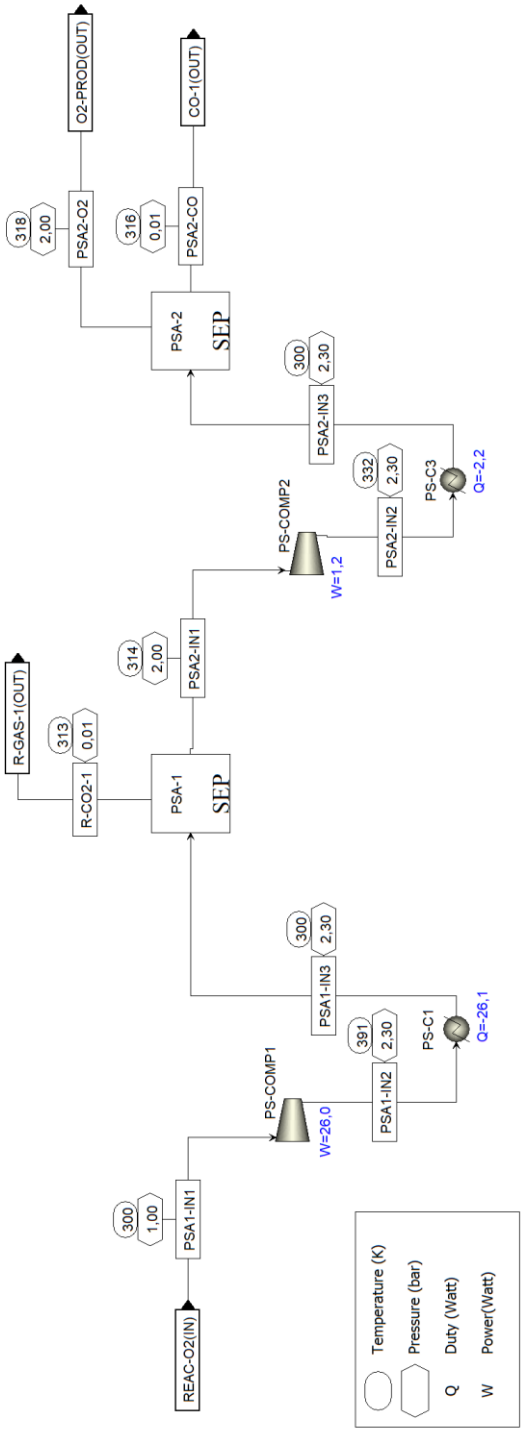

B) Detailed Summary of Simulation Results for an Exemplary Operating Point

Stream Name		FEED-1	DRY-1	WATER	REAC-I1	REAC-O1	REAC-O2	PSA1-IN1	PSA1-IN2	PSA1-IN3	R-CO2-1	R-GAS-1
Temperature	C	25.0	25.0	25.0	25.0	800.0	26.9	26.9	98.5	26.9	39.9	39.9
Pressure	bar	1.00	1.00	1.00	1.00	1.00	1.00	1.00	2.30	2.30	0.01	0.01
Molar Enthalpy	$\frac{kJ}{mol}$	-386.2	-386.2	-357.5	-387.3	-261.1	-294.4	-294.4	-291.9	-294.5	-387.0	-387.0
Molar Entropy	$\frac{J}{mol * K}$	4	4	-51	5	80	27	27	28	20	45	45
Molar Density	$\frac{mol}{m^3}$	40.56	40.56	59.24	40.56	11.20	40.23	40.23	74.71	92.96	0.38	0.38
Mass Density	$\frac{kg}{m^3}$	1.776	1.776	2.094	1.774	0.442	1.588	1.588	2.950	3.670	0.017	0.017
Enthalpy Flow	W	-600	-600	0	-2736	-2043	-2304	-2304	-2284	-2304	-2133	-2133
Mole Flows	$\frac{mmol}{s}$	1.55380	1.55267	0.00113	7.06362	7.82550	7.82550	7.82550	7.82550	7.82550	5.51095	5.51095
O2	$\frac{mmol}{s}$	0.02891	0.02891	0	0.05647	0.81834	0.81834	0.81834	0.81834	0.81834	0.02755	0.02755
CO	$\frac{mmol}{s}$	0	0	0	0.07715	1.60091	1.60091	1.60091	1.60091	1.60091	0.07715	0.07715
CO2	$\frac{mmol}{s}$	1.52451	1.52375	0.00076	6.93000	5.40625	5.40625	5.40625	5.40625	5.40625	5.40625	5.40625
H2O	$\frac{mmol}{s}$	0.00038	0	0.00038	0	0	0	0	0	0	0	0
Mole Fractions												
O2	-	0.01861	0.01862	0	0.00799	0.10457	0.10457	0.10457	0.10457	0.10457	0.00500	0.00500
CO	-	0	0	0	0.01092	0.20458	0.20458	0.20458	0.20458	0.20458	0.01400	0.01400
CO2	-	0.98115	0.98138	0.66667	0.98108	0.69085	0.69085	0.69085	0.69085	0.69085	0.98100	0.98100
H2O	-	0.00024	0	0.33333	0	0	0	0	0	0	0	0
Volume Flow	$\frac{l}{s}$	0.038	0.038	0.000	0.174	0.698	0.195	0.195	0.105	0.084	14.341	14.341

Stream Name		R-GAS-2	R-GAS-3	R-GAS-4	R-GAS-5	PSA2-IN1	PSA2-IN2	PSA2-IN3	PSA2-O2	O2-PROD	PSA2-CO	CO-1
Temperature	C	246.3	40.0	246.6	25.0	40.9	55.3	26.9	44.9	44.9	42.9	42.9
Pressure	bar	0.10	0.10	1.00	1.00	2.00	2.30	2.30	2.00	2.00	0.01	0.01
Molar Enthalpy	$\frac{\text{kJ}}{\text{mol}}$	-378.4	-387.0	-378.4	-387.6	-72.3	-71.9	-72.7	-3.6	-3.6	-108.6	-108.6
Molar Entropy	$\frac{\text{J}}{\text{mol} * \text{K}}$	47	26	28	5	60	60	57	1	1	129	129
Molar Density	$\frac{\text{mol}}{\text{m}^3}$	2.32	3.84	23.15	40.56	76.67	84.30	92.33	75.75	75.75	0.38	0.38
Mass Density	$\frac{\text{kg}}{\text{m}^3}$	0.101	0.168	1.012	1.773	2.252	2.476	2.712	2.413	2.413	0.011	0.011
Enthalpy Flow	W	-2085	-2133	-2085	-2136	-167	-166	-168	-3	-3	-164	-164
Mole Flows	$\frac{\text{mmol}}{\text{s}}$	5.51095	5.51095	5.51095	5.51095	2.31454	2.31454	2.31454	0.80144	0.80144	1.51310	1.51310
O2	$\frac{\text{mmol}}{\text{s}}$	0.02755	0.02755	0.02755	0.02755	0.79079	0.79079	0.79079	0.77157	0.77157	0.01922	0.01922
CO	$\frac{\text{mmol}}{\text{s}}$	0.07715	0.07715	0.07715	0.07715	1.52375	1.52375	1.52375	0.02987	0.02987	1.49389	1.49389
CO2	$\frac{\text{mmol}}{\text{s}}$	5.40625	5.40625	5.40625	5.40625	0	0	0	0	0	0	0
H2O	$\frac{\text{mmol}}{\text{s}}$	0	0	0	0	0	0	0	0	0	0	0
Mole Fractions												
O2	-	0.00500	0.00500	0.00500	0.00500	0.34166	0.34166	0.34166	0.96274	0.96274	0.01270	0.01270
CO	-	0.01400	0.01400	0.01400	0.01400	0.65834	0.65834	0.65834	0.03726	0.03726	0.98730	0.98730
CO2	-	0.98100	0.98100	0.98100	0.98100	0	0	0	0	0	0	0
H2O	-	0	0	0	0	0	0	0	0	0	0	0
Volume Flow	$\frac{\text{l}}{\text{s}}$	2.380	1.434	0.238	0.136	0.030	0.027	0.025	0.011	0.011	3.975	3.975

Stream Name		CO-2	CO-3	CO-4	CO-5	CO-6	CO-PROD
Temperature	C	173.5	40.0	242.7	40.0	413.1	150.0
Pressure	bar	0.03	0.03	0.15	0.15	2.00	2.00
Molar Enthalpy	$\frac{\mathrm{kJ}}{\mathrm{mol}}$	-104.8	-108.7	-102.7	-108.7	-97.5	-105.5
Molar Entropy	$\frac{\mathrm{J}}{\mathrm{mol} * \mathrm{K}}$	130	119	121	106	108	93
Molar Density	$\frac{\mathrm{mol}}{\mathrm{m}^3}$	0.81	1.15	3.50	5.76	35.02	56.82
Mass Density	$\frac{\mathrm{kg}}{\mathrm{m}^3}$	0.023	0.032	0.098	0.162	0.983	1.594
Enthalpy Flow	W	-159	-164	-155	-164	-148	-160
Mole Flows	$\frac{\mathrm{mmol}}{\mathrm{s}}$	1.51310	1.51310	1.51310	1.51310	1.51310	1.51310
O2	$\frac{\mathrm{mmol}}{\mathrm{s}}$	0.01922	0.01922	0.01922	0.01922	0.01922	0.01922
CO	$\frac{\mathrm{mmol}}{\mathrm{s}}$	1.49389	1.49389	1.49389	1.49389	1.49389	1.49389
CO2	$\frac{\mathrm{mmol}}{\mathrm{s}}$	0	0	0	0	0	0
H2O	$\frac{\mathrm{mmol}}{\mathrm{s}}$	0	0	0	0	0	0
Mole Fractions							
O2	-	0.01270	0.01270	0.01270	0.01270	0.01270	0.01270
CO	-	0.98730	0.98730	0.98730	0.98730	0.98730	0.98730
CO2	-	0	0	0	0	0	0
H2O	-	0	0	0	0	0	0
Volume Flow	$\frac{\mathrm{l}}{\mathrm{s}}$	1.873	1.313	0.433	0.263	0.043	0.027

C) Summary of Main Technological Results of all Evaluated Operating Points | Case A

Operating Point Number	Reactor Inlet Flow	Conversion Rate	SEI Plasma	Total Efficiency	Total EPC	PSA Compressor	Product Compressor	Recycle Compressor	MW Plasma Reactor
	$\frac{\text{mmol}}{\text{s}}$	%	$\frac{\text{kJ}}{\text{mol}}$	%	$\frac{\text{kWh}}{\text{Nm}^3}$	W	W	W	W
1	2.77	56.63	974.5	11.10	31.60	10.48	32.99	21.27	3856.1
2	3.46	55.38	779.6	13.51	25.95	13.00	40.29	27.33	3853.3
3	2.77	54.70	866.2	12.04	29.13	10.37	31.86	22.21	3427.6
4	2.77	54.28	812.1	12.73	27.56	10.34	31.61	22.42	3213.4
5	2.77	54.16	757.9	13.59	25.81	10.34	31.55	22.48	2999.2
6	3.46	53.08	693.0	14.54	24.13	12.83	38.62	28.74	3425.2
7	2.77	52.91	703.8	14.27	24.58	10.27	30.82	23.09	2785.0
8	2.77	51.01	649.6	14.88	23.57	10.16	29.71	24.02	2570.7
9	3.46	50.37	606.3	15.72	22.32	12.64	36.64	30.40	2997.0
10	2.77	48.22	595.5	15.31	22.90	10.00	28.09	25.39	2356.5
11	3.46	48.04	563.0	16.11	21.77	12.47	34.95	31.83	2783.0
12	3.46	45.17	519.7	16.38	21.42	12.27	32.86	33.59	2568.9
13	2.77	44.81	541.4	15.62	22.46	9.80	26.10	27.06	2142.3
14	3.46	42.24	476.4	16.67	21.04	12.06	30.73	35.38	2354.8
15	2.77	41.13	487.2	15.88	22.08	9.59	23.96	28.87	1928.1
16	3.46	38.76	433.1	16.78	20.91	11.81	28.20	37.57	2140.7
17	2.77	37.56	433.1	16.26	21.58	9.39	21.88	30.62	1713.8
18	3.46	35.05	389.8	16.79	20.89	11.55	25.50	39.91	1926.7
19	6.93	34.62	389.8	16.59	21.15	23.07	50.39	80.46	3858.9
20	6.93	34.38	389.8	16.48	21.29	23.03	50.05	80.75	3858.9
21	2.77	33.57	379.0	16.53	21.22	9.16	19.55	32.58	1499.6
22	3.46	31.15	346.5	16.72	20.98	11.27	22.66	42.30	1712.6
23	6.93	30.94	346.5	16.60	21.13	22.54	45.08	84.99	3430.1
24	6.93	30.77	346.5	16.51	21.24	22.52	44.84	85.20	3430.1
25	2.77	29.38	324.8	16.78	20.91	8.92	17.17	34.63	1285.4
26	3.46	27.46	303.2	16.75	20.94	11.01	19.98	44.57	1498.5
27	6.93	27.46	303.2	16.75	20.94	22.05	40.01	89.27	3001.4
28	6.93	27.36	303.2	16.68	21.02	22.03	39.86	89.40	3001.4
29	3.46	23.83	259.9	16.83	20.85	10.75	17.39	46.80	1284.4
30	6.93	23.82	259.9	16.83	20.85	21.53	34.72	93.74	2572.6
31	6.93	23.59	259.9	16.66	21.05	21.50	34.38	94.03	2572.6

32	10.40	22.75	259.9	16.07	21.82	32.08	49.71	142.66	3860.7
33	10.40	22.75	259.9	16.07	21.83	32.08	49.69	142.67	3860.7
34	6.93	21.99	238.2	16.86	20.80	21.27	32.04	96.00	2358.2
35	6.93	21.76	238.2	16.69	21.02	21.23	31.71	96.28	2358.2
36	10.40	20.08	231.0	15.85	22.12	31.51	43.91	147.60	3431.8
37	6.93	20.05	216.5	16.82	20.86	20.99	29.22	98.39	2143.8
38	10.40	20.01	231.0	15.80	22.20	31.49	43.76	147.73	3431.8
39	6.93	19.82	216.5	16.62	21.10	20.96	28.88	98.67	2143.8
40	6.93	18.13	194.9	16.78	20.90	20.72	26.42	100.74	1929.4
41	6.93	17.87	194.9	16.54	21.20	20.68	26.04	101.07	1929.4
42	10.40	17.66	202.1	15.80	22.20	30.99	38.61	152.07	3002.8
43	10.40	17.59	202.1	15.74	22.29	30.98	38.46	152.20	3002.8
44	13.90	16.35	194.9	15.14	23.17	41.05	47.73	206.48	3870.0
45	6.93	16.19	173.2	16.72	20.98	20.44	23.60	103.13	1715.1
46	6.93	15.98	173.2	16.50	21.26	20.41	23.28	103.40	1715.1
47	10.40	15.32	173.2	15.82	22.18	30.49	33.49	156.39	2573.8
48	10.40	15.20	173.2	15.70	22.34	30.47	33.24	156.60	2573.8
49	13.90	14.69	173.2	15.17	23.11	40.58	42.94	210.56	3440.0
50	6.93	14.24	151.6	16.63	21.10	20.17	20.75	105.53	1500.7
51	6.93	14.04	151.6	16.39	21.40	20.14	20.46	105.78	1500.7
52	10.40	14.04	158.8	15.71	22.33	30.22	30.70	158.75	2359.3
53	13.90	12.97	151.6	15.14	23.16	40.09	37.90	214.82	3010.0
54	10.40	12.82	144.4	15.65	22.41	29.96	28.04	161.00	2144.9
55	10.40	12.77	144.4	15.59	22.50	29.95	27.92	161.10	2144.9
56	6.93	12.29	129.9	16.50	21.26	19.89	17.96	107.94	1286.3
57	6.93	12.11	129.9	16.26	21.57	19.86	17.70	108.16	1286.3
58	10.40	11.56	129.9	15.53	22.59	29.69	25.29	163.32	1930.4
59	13.90	11.33	129.9	15.21	23.06	39.62	33.11	218.87	2580.0
60	13.90	10.50	119.1	15.25	23.00	39.38	30.70	220.91	2365.0
61	10.40	10.33	115.5	15.42	22.74	29.43	22.60	165.60	1715.9
62	10.40	10.24	115.5	15.29	22.94	29.41	22.40	165.76	1715.9
63	13.90	9.65	108.3	15.24	23.01	39.14	28.19	223.02	2150.0
64	10.40	9.11	101.1	15.29	22.94	29.17	19.91	167.86	1501.4
65	13.90	8.76	97.4	15.19	23.10	38.89	25.60	225.21	1935.0
66	13.90	7.88	86.6	15.13	23.18	38.64	23.04	227.38	1720.0

D) Summary of Main Technological Results of all Evaluated Operating Points | Case B

Operating Point Number	Reactor Inlet Flow	Conversion Rate	SEI Plasma	Total Efficiency	Total EPC	PSA Compressor	Product Compressor	Recycle Compressor	MW Plasma Reactor
	$\frac{mmol}{s}$	%	$\frac{kJ}{mol}$	%	$\frac{kWh}{Nm^3}$	W	W	W	W
1	2.77	56.63	974.5	11.40	30.77	10.48	32.99	21.27	3753.7
2	3.46	55.38	779.6	13.90	25.23	13.00	40.29	27.33	3744.0
3	2.77	54.70	866.2	12.03	29.15	10.37	31.86	22.21	3429.8
4	2.77	54.28	812.1	12.56	27.92	10.34	31.61	22.42	3256.7
5	2.77	54.16	757.9	13.23	26.52	10.34	31.55	22.48	3082.8
6	3.46	53.08	693.0	14.54	24.13	12.83	38.62	28.74	3425.5
7	2.77	52.91	703.8	13.67	25.66	10.27	30.82	23.09	2911.2
8	2.77	51.01	649.6	14.00	25.05	10.16	29.71	24.02	2736.5
9	3.46	50.37	606.3	15.27	22.96	12.64	36.64	30.40	3085.9
10	2.77	48.22	595.5	14.11	24.85	10.00	28.09	25.39	2562.3
11	3.46	48.04	563.0	15.43	22.74	12.47	34.95	31.83	2910.1
12	3.46	45.17	519.7	15.41	22.76	12.27	32.86	33.59	2734.6
13	2.77	44.81	541.4	14.04	24.98	9.80	26.10	27.06	2390.0
14	3.46	42.24	476.4	15.37	22.82	12.06	30.73	35.38	2560.4
15	2.77	41.13	487.2	13.85	25.32	9.59	23.96	28.87	2219.7
16	3.46	38.76	433.1	15.09	23.24	11.81	28.20	37.57	2388.3
17	2.77	37.56	433.1	13.66	25.67	9.39	21.88	30.62	2050.9
18	3.46	35.05	389.8	14.66	23.92	11.55	25.50	39.91	2218.1
19	6.93	34.62	389.8	17.06	20.56	23.07	50.39	80.46	3748.3
20	6.93	34.38	389.8	16.91	20.75	23.03	50.05	80.75	3756.4
21	2.77	33.57	379.0	13.27	26.42	9.16	19.55	32.58	1882.3
22	3.46	31.15	346.5	14.07	24.93	11.27	22.66	42.30	2049.4
23	6.93	30.94	346.5	16.58	21.16	22.54	45.08	84.99	3435.9
24	6.93	30.77	346.5	16.48	21.28	22.52	44.84	85.20	3436.8
25	2.77	29.38	324.8	12.74	27.53	8.92	17.17	34.63	1711.6
26	3.46	27.46	303.2	13.48	26.03	11.01	19.98	44.57	1880.9
27	6.93	27.46	303.2	16.29	21.54	22.05	40.01	89.27	3090.4
28	6.93	27.36	303.2	16.23	21.62	22.03	39.86	89.40	3090.4
29	3.46	23.83	259.9	12.81	27.38	10.75	17.39	46.80	1710.4
30	6.93	23.82	259.9	15.86	22.12	21.53	34.72	93.74	2738.5
31	6.93	23.59	259.9	15.70	22.33	21.50	34.38	94.03	2738.5

32	10.40	22.75	259.9	16.48	21.28	32.08	49.71	142.66	3759.3
33	10.40	22.75	259.9	16.49	21.28	32.08	49.69	142.67	3757.0
34	6.93	21.99	238.2	15.58	22.51	21.27	32.04	96.00	2564.1
35	6.93	21.76	238.2	15.42	22.75	21.23	31.71	96.28	2564.1
36	10.40	20.08	231.0	15.82	22.16	31.51	43.91	147.60	3438.5
37	6.93	20.05	216.5	15.18	23.11	20.99	29.22	98.39	2391.7
38	10.40	20.01	231.0	15.77	22.24	31.49	43.76	147.73	3438.5
39	6.93	19.82	216.5	15.00	23.38	20.96	28.88	98.67	2391.7
40	6.93	18.13	194.9	14.72	23.83	20.72	26.42	100.74	2221.3
41	6.93	17.87	194.9	14.50	24.18	20.68	26.04	101.07	2221.3
42	10.40	17.66	202.1	15.38	22.81	30.99	38.61	152.07	3091.9
43	10.40	17.59	202.1	15.32	22.90	30.98	38.46	152.20	3091.9
44	13.90	16.35	194.9	15.52	22.60	41.05	47.73	206.48	3767.2
45	6.93	16.19	173.2	14.16	24.78	20.44	23.60	103.13	2052.4
46	6.93	15.98	173.2	13.97	25.12	20.41	23.28	103.40	2052.4
47	10.40	15.32	173.2	14.93	23.49	30.49	33.49	156.39	2739.8
48	10.40	15.20	173.2	14.82	23.67	30.47	33.24	156.60	2739.8
49	13.90	14.69	173.2	15.15	23.16	40.58	42.94	210.56	3446.7
50	6.93	14.24	151.6	13.49	26.00	20.17	20.75	105.53	1883.6
51	6.93	14.04	151.6	13.30	26.38	20.14	20.46	105.78	1883.6
52	10.40	14.04	158.8	14.54	24.12	30.22	30.70	158.75	2565.4
53	13.90	12.97	151.6	14.74	23.79	40.09	37.90	214.82	3099.3
54	10.40	12.82	144.4	14.17	24.76	29.96	28.04	161.00	2392.9
55	10.40	12.77	144.4	14.11	24.86	29.95	27.92	161.10	2392.9
56	6.93	12.29	129.9	12.71	27.59	19.89	17.96	107.94	1712.9
57	6.93	12.11	129.9	12.53	27.99	19.86	17.70	108.16	1712.9
58	10.40	11.56	129.9	13.67	25.66	29.69	25.29	163.32	2222.4
59	13.90	11.33	129.9	14.38	24.39	39.62	33.11	218.87	2746.4
60	13.90	10.50	119.1	14.15	24.79	39.38	30.70	220.91	2571.5
61	10.40	10.33	115.5	13.13	26.71	29.43	22.60	165.60	2053.3
62	10.40	10.24	115.5	13.02	26.95	29.41	22.40	165.76	2053.3
63	13.90	9.65	108.3	13.83	25.35	39.14	28.19	223.02	2398.6
64	10.40	9.11	101.1	12.50	28.05	29.17	19.91	167.86	1884.5
65	13.90	8.76	97.4	13.42	26.14	38.89	25.60	225.21	2227.7
66	13.90	7.88	86.6	12.95	27.08	38.64	23.04	227.38	2058.3

E) Total Purchased Equipment Cost Calculation Spreadsheet

Equipment	Total required size	Maximum size	Number of trains	Sizing parameter	Equipments per train	Total number of equipments	Purchased equipment cost	Reference
Dryer	214 m^3	150 m^3	2	107	2	4	0.329 €	[42]
MW plasma reactor	1647 MW	100 kW	16467	100	1	16467	2305 €	[3]
PSA 1 columns	7070 m^3	300 m^3	24	295	4	96	19.50 €	[42]
PSA 2 columns	1457 m^3	300 m^3	5	291	4	20	4.021 €	[42]
PSA 1 compressor	15.3 MW	10000 kW	2	7624	1	2	3.550 €	[42, 44]
PSA 2 compressor	682 kW	10000 kW	1	682	1	1	0.26 €	[42, 44]
Recycle compressor	68.0 MW	10000 kW	7	9716	1	7	15.09 €	[42, 44]
Product compressor	22.9 MW	10000 kW	3	7643	1	3	5.336 €	[42, 44]
Gas cooler	371 m^2	1050 m^2	1	1021	1	1	0.234 €	[42]
Turbine-Generator set (incl. HRSG)	66.3 MW	100000 kW	1	66285	1	1	30.76 €	[42, 44, 53, 54]

F) Detailed Single-variable Sensitivity Diagrams